Manuscript prepared for Biogeosciences
with version 5.0 of the LaTeX class copernicus.cls.
Date: 30 November 2015

# Data-based estimates of the ocean carbon sink variability – First results of the Surface Ocean $p\mathrm{CO_2}$ Mapping intercomparison (SOCOM)

**C. Rödenbeck[1], D.C.E. Bakker[2], N. Gruber[3], Y. Iida[4], A.R. Jacobson[5], S. Jones[6], P. Landschützer[3], N. Metzl[7], S. Nakaoka[8], A. Olsen[9], G.-H. Park[10], P. Peylin[11], K.B. Rodgers[12], T.P. Sasse[13], U. Schuster[6], J.D. Shutler[6], V. Valsala[14], R. Wanninkhof[15], and J. Zeng[8]**

[1]Max Planck Institute for Biogeochemistry, Jena, Germany
[2]Centre for Ocean and Atmospheric Sciences, School of Environmental Sciences, University of East Anglia, Norwich, UK
[3]Institute for Biogeochemistry and Pollutant Dynamics, ETH Zürich, Zürich, Switzerland
[4]Global Environment and Marine Department, Japan Meteorological Agency, Tokyo, Japan
[5]University of Colorado and NOAA Earth System Research Laboratory, Boulder Colorado, USA
[6]College of Life and Environmental Sciences, University of Exeter, UK
[7]Sorbonne Universités (UPMC, Univ Paris 06)-CNRS-IRD-MNHN, LOCEAN/IPSL Laboratory, Paris, France
[8]National Institute for Environmental Studies, Tsukuba, Japan
[9]Geophysical Institute, University of Bergen and Bjerknes Centre for Climate Research, Bergen, Norway
[10]East Sea Research Institute, Korea Institute of Ocean Science and Technology, Uljin, Republic of Korea
[11]Laboratoire des Sciences du Climat et de l'Environnement (LSCE), Gif sur Yvette, France
[12]Atmospheric and Oceanic Sciences Program, Princeton University, NJ, USA
[13]Climate Change Research Centre, University of New South Wales, Sydney, Australia
[14]Indian Institute of Tropical Meteorology, Pune, India
[15]NOAA Atlantic Oceanographic and Meteorological Laboratory, Miami Florida, USA

**Abstract.** Using measurements of the surface-ocean $\mathrm{CO_2}$ partial pressure ($p\mathrm{CO_2}$) and 14 different $p\mathrm{CO_2}$ mapping methods recently collated by the Surface Ocean $p\mathrm{CO_2}$ Mapping intercomparison (SOCOM) initiative, variations in regional and global sea–air $\mathrm{CO_2}$ fluxes are investigated. Though the available mapping methods use widely different approaches, we find relatively consistent estimates of regional $p\mathrm{CO_2}$ seasonality, in line with previous estimates. In terms of interannual variability (IAV), all mapping methods estimate the largest variations to occur in the Eastern equatorial Pacific. Despite considerable spread in the detailed variations, mapping methods that fit the data more closely also tend to agree more closely with each other in regional averages. Encouragingly, this includes mapping methods belonging to complementary types – taking variability either directly from the $p\mathrm{CO_2}$ data or indirectly from driver data via regression. From a weighted ensemble average, we find an IAV amplitude of the global sea–air $\mathrm{CO_2}$ flux of $0.31\,\mathrm{PgC\,yr^{-1}}$ (standard deviation over 1992–2009), which is larger than simulated by biogeochemical process models. On a decadal perspective, the global ocean $\mathrm{CO_2}$ uptake is estimated to have gradually increased since about 2000, with little decadal change prior to that. The weighted mean net global ocean $\mathrm{CO_2}$ sink estimated by the SOCOM ensemble is $-1.75\,\mathrm{PgC\,yr^{-1}}$ (1992–2009), consistent within uncertainties with estimates from ocean-interior carbon data or atmospheric oxygen trends.

## 1 Introduction

The global ocean acts as a major sink for anthropogenic carbon, and thereby helps to slow down the human-induced warming of the Earth's climate (Stocker et al., 2013). Presently, approximately 27% of the annually emitted carbon is taken up by the ocean (Le Quéré et al., 2015); in total 30% of the anthropogenic carbon emitted since the industrialization of our planet has been stored by the ocean (Sabine et al., 2004; Khatiwala et al., 2013). Thus, variations in the oceanic carbon sink, in particular a possible decline under

climate change, co-determine the future climate trajectory. In addition to this direct relevance, present-day variations in the sea–air $CO_2$ exchange, when related to possible driving factors, can be employed to provide information on the underlying mechanisms of ocean biogeochemistry.

Until recently, estimates of the oceanic $CO_2$ uptake rate and its variability were largely based on (1) ocean biogeochemical process models (see, e.g., Wanninkhof et al., 2013), (2) inverse estimates based on atmospheric $CO_2$ data (see Peylin et al., 2013), or (3) inverse estimates based on ocean-interior carbon data (Gloor et al., 2003, and subsequent refinements). However, while process models are useful tools to study the sensitivity of carbon fluxes to the physical and biogeochemical mechanisms that control them, they are not specifically designed for state estimation and thus have large uncertainties if used in this way (Wanninkhof et al., 2013). Likewise, while atmospheric $CO_2$ inversions are able to provide estimates of land–air $CO_2$ exchange on large scales, their sea–air $CO_2$ flux estimates suffer from large relative errors over most of the ocean due to the dominance of land variability in the atmospheric signals (Peylin et al., 2013). Finally, while ocean-interior inversions offer a strong data-based constraint on the long-term flux in larger regions, they do not provide flux variability or finer spatial detail.

A more direct quantification of the sea–air $CO_2$ flux is possible using measurements of the oceanic and atmospheric partial pressures of $CO_2$ ($pCO_2$) in conjunction with a parameterization of the gas transfer across the sea–air interface. Through extensive concerted community efforts, more than 10 million surface ocean $pCO_2$ measurements were gathered and recently compiled into the SOCATv2 (Surface Ocean $CO_2$ Atlas version 2, Bakker et al., 2014) and the LDEOv2013 (Lamont-Doherty Earth Observatory version 2013, Takahashi et al., 2014a) databases.

Although $pCO_2$ data are thus available in nearly all ocean basins for several decades, observations from ships or fixed sensors can necessarily only cover a tiny fraction of the spatio-temporal $pCO_2$ field of the global surface ocean. Therefore, to obtain continuous sea–air $CO_2$ flux fields over larger areas or the entire ocean, interpolation (gap-filling) methods are needed to estimate values in all the periods and areas not directly observed. Various methods have been proposed to interpolate $pCO_2$ data in space and time (Appendix A). They span a wide range of approaches, in particular with respect to the information sources tapped and assumptions imposed. Due to that, some methods are able to reproduce the signals in the data more closely while others are able to bridge the data-void areas/periods more effectively (Fig. 1).

These complementary characteristics of the various approaches to some degree reflect differing targets of the individual studies. Correspondingly, their strengths and weaknesses can be expected to vary depending on the given purpose. However, this complementarity offers a great opportunity for robustness assessment, as the existence of common features in the results of mapping methods based on different principles give strong support to the estimates. In periods or areas without data, this is the only available way to assess uncertainties. Further, we can investigate the information content of the various data streams used by some methods and not used by others. It is the primary objective of the Surface Ocean $pCO_2$ Mapping intercomparison (SOCOM) initiative to foster such inter-method investigations. SOCOM is not meant to rank methods but to exploit the added value of their complementarity. Ultimately it aims to identify which features of the surface-ocean $pCO_2$ field (and consequently the sea–air $CO_2$ flux) can be robustly inferred from the available surface-ocean carbon data, and to provide quantitative estimates for these features, including an uncertainty assessment. These sea–air $CO_2$ flux estimates based on surface-ocean carbon data are then available to feed into comprehensive carbon cycle syntheses like the REgional Carbon Cycle Assessment and Processes (RECCAP) activity of the Global Carbon Project (http://www.globalcarbonproject.org/reccap/), which until recently mainly had to rely on model simulations for variability.

This paper first introduces the ensemble of data-driven $pCO_2$ mapping methods currently available in the SOCOM initiative (Sect. 2), and gives an overview of the estimated seasonality and interannual variability (IAV) in oceanic "biomes" (Sect. 4.1). As some of these $pCO_2$ data-driven methods have been used to assess interannual variations of global sea–air $CO_2$ fluxes in recent carbon budgets by the Global Carbon Project (GCP) (Le Quéré et al., 2015), we then specifically analyse the interannual variations in the sea–air $CO_2$ fluxes. Focus is put on the consistency between regressing and non-regressing methods, and on the amplitude of the interannual sea–air $CO_2$ flux variability (Sect. 4.2).

## 2 Mapping Methods

This section provides an overview of the principles of the various mapping approaches, and the range of particular choices taken within each method class. Details on the individual mapping methods (referenced by labels in italics) are given in Appendix A and the references cited there. Essential properties and technical parameters are summarized in Tables 1–3. In particular, Table 3 gives the spatial and temporal coherence scales of the adjustible degrees of freedom, determining the balance between the ability of a method to bridge data gaps and its ability to directly follow the observed signals (see table footnote $e$). Table 4 indicates which modes of $pCO_2$ variability are, by construction of the individual methods, estimated from the $pCO_2$ data information (rather than prescribed or determined in other ways). For a summary of method classes see Fig. 1 and its caption.

### 2.1 Statistical interpolation

Statistical interpolation schemes fit the data to suitable auto-regressive models. The applied auto-correlation scales have either been determined from the $pCO_2$ data themselves (*UEA-SI*, *OceanFlux-SI*), chosen to reflect data density (*Jena-MLS*), or derived from empirical orthogonal function (EOF) analysis of an ensemble of process model simulations (*CU-SCSE*). The interpolation is either done directly for the $pCO_2$ field (*UEA-SI*, *OceanFlux-SI*, *CU-SCSE*) or indirectly for the field of ocean-internal carbon sources and sinks determining the $pCO_2$ field (*Jena-MLS*).

In most statistical interpolation schemes, those pixels/timesteps that are neither directly constrained by co-located data, nor indirectly constrained by sufficiently close data (within the spatial or temporal correlation scales), fall back to some "background state" or "prior", namely: the estimated mean seasonality and estimated trend (*UEA-SI*), parametrized temperature-related variations (*Jena-MLS*), or a prescribed climatology plus a prescribed linear trend (*CU-SCSE*). The ordinary block kriging used in *OceanFlux-SI* does not use a-priori data values and interpolates the data to any distance, though the estimation uncertainty increases with interpolation distance.

### 2.2 Regression to external drivers

#### 2.2.1 Linear Regression

(Multi-)linear regression (*AOML-EMP*, *UEx-MLR*, *JMA-MLR*) expresses $pCO_2$ as a linear combination of a set of one or more driving variables (such as Sea Surface Temperature (SST), Sea Surface Salinity (SSS), Mixed-layer depth (MLD), Chlorophyll-a, etc.), and adjusts their multipliers as to best match the $pCO_2$ observations. The calculation is done separately for each of a set of spatio-temporal domains. Individual implementations differ in the set of chosen driver variables, as well as in the choice of spatio-temporal domains over which the same adjustable multipliers are used.

#### 2.2.2 Non-linear Regression

The forms of non-linear regression technique currently applied to map the sea surface $pCO_2$ are self–organizing maps (SOM) (*NIES-SOM*) and feed-forward networks (FFN) (*NIES-NN*, *CARBONES-NN*), as well as combinations of SOM and FFN (*ETH-SOMFFN*) or SOM and linear regression (*UNSW-SOMLO*).

- Self-organizing maps (SOM) project (multi-dimensional) driver variables to a two-dimensional discrete space of clusters ("neuron cells"). Observed $pCO_2$ values are then assigned to the clusters according to their associated driver variable values. With this information, spatio-temporal $pCO_2$ maps are created by finding neuron cells with similar driver variable values for any given location/timestep, and using the associated $pCO_2$ value there.
- Feed-forward networks (FFN) establish a statistical non-linear relationship between a set of driver variables and $pCO_2$ observations (training), and apply this relationship to continuous fields of the driver variables to create a continuous $pCO_2$ map (prediction).

As for linear regression, the individual implementations differ in the set of chosen physical or biogeochemical driver variables (SST, SSS, MLD, Chl-a, etc.). Different choices have also been made concerning spatialization: While some implementations use independent neural networks within predefined spatial or spatio-temporal regions, others use one global network but add spatial or temporal coordinate variables to the set of drivers.

Non-linear regression methods have the advantage over linear regressions that they can flexibly represent a wide class of $pCO_2$–driver relationships. On the other hand, FFNs involve the risk that the non-linear extrapolation into data-sparse regions becomes unstable and produces outliers. SOMs avoid this risk, though instead their discrete output may contain spatial discontinuities.

### 2.3 Model-based Regression and Tuning

Although biogeochemical simulation models can successfully be tuned to reproduce WOCE-era transient tracer inventories (Matsumoto et al., 2004), this does not assure skill in simulating trends and interannual variability, as tuning itself can in some instances merely be compensating for improper process representation or insufficient parameterizations. Data assimilation or non-linear inverse modeling efforts such as ECCO have been demonstrated to improve the representation of the evolving physical state of the ocean (Wunsch et al., 2009). Although promising, the incorporation of biogeochemistry into a consistent assimilation or inversion framework is still in the early stages of development.

Within the methods collated here, biogeochemical ocean process models have been used in the following ways:

- Modelled $pCO_2$ fields have been split into different time scales (seasonality, interannual variations) and scaled as to optimally match the $pCO_2$ data (*PU-MCMC*).
- Boundary conditions and initial fields of Dissolved Inorganic Carbon (DIC) are tuned during the model run itself as to optimally match the $pCO_2$ data (*NIES-OTTM*).

## 3 Analysis Methods

### 3.1 Ensemble collection

The $pCO_2$ fields estimated by the various methods were regridded by each provider to a resolution of $1^\circ$ latitude $\times 1^\circ$

longitude and monthly time steps, preferably by averaging (if the original resolution is higher) or sub-sampling (if the original resolution is lower). Also a sea-mask (map of covered ocean area, possibly fractional) was requested from each provider. All subsequent processing was done by common scripts.

### 3.2 Spatial gap filling

Most methods do not cover the entire ocean surface (see Fig. A6). In particular, coastal areas or the Arctic are excluded in many methods. Some methods depending on satellite-derived Chlorophyll-a input data exclude some high-latitude areas during the dark season. *OceanFlux-SI* misses all locations/months where the satellite-derived SST input data are invalid. *UEx-MLR* has occasional invalid pixels due to numerical reasons.

These invalid pixels would pose severe problems to the ensemble analysis because (1) spatial averages (Sect. 3.3) would not extend over the same area, causing spurious differences between the methods, and (2) the calculated sea-air $CO_2$ fluxes (Sect. 3.6) would miss parts of the ocean. Restricting the comparison to the common ocean surface would only partially solve (1) and not solve (2).

Therefore, we filled any pixels in the $pCO_2$ maps that are not covered by the considered mapping method (according to its sea mask or its value being outside $0 < pCO_2 < 10^6 \mu\mathrm{atm}$) but are ocean (according to bathymetry taken from the ETOPO surface elevation data (U.S. Department Commerce, 2006, access date 02/03/2011)) by a common standard $pCO_2$ field. This standard field is the sum of the monthly climatology by Takahashi et al. (2014b) plus the year-to-year atmospheric $pCO_2$ increase (the year-to-year atmospheric $pCO_2$ increase is derived from observed atmospheric $CO_2$ mixing ratios by the Jena $CO_2$ inversion s85_v3.5 (as in Rödenbeck et al. (2013)); we use a 12-month running mean of the atmospheric $pCO_2$ minus its mean in 2005, the year of the Takahashi et al. (2014b) climatology). The filled pixels do not change the results strongly compared to signal size.

### 3.3 Biome averages

In this overview of the ensemble of mapping methods, we consider time series of $pCO_2$ averaged over the 17 biomes of Fay and McKinley (2014) (Fig. 2, Table 5). We use the time-independent "mean biomes", such that no spurious common variability can be induced from changing averaging domains. These biomes were chosen as they were derived from coherence in sea surface temperature (SST), spring/summer chlorophyll a concentrations (Chl-a), ice fraction, and maximum mixed layer depth, and thus may reflect areas of relatively coherent biogeochemical behaviour better than previously used "rectangular" regions (e.g., RECCAP, TransCom). To filter for interannual variations (IAV), we consider 12-month running means.

### 3.4 Time periods

Results are plotted over the respective valid period of each method. Statistical analyses are restricted to the 1992–2009 period, when results of most mapping methods are available, and when the data coverage is relatively good (this refers in particular to the Equatorial Pacific).

### 3.5 Diagnostics – comparison to data

#### 3.5.1 Mismatch time series

As a 1st order performance diagnostic, we compare the mapping results to the monthly observed values in the SOCATv2 gridded product (Sabine et al., 2013; Bakker et al., 2014) (unweighted averages – variable FCO2_AVE_UNWTD of file "SOCAT_tracks_gridded_monthly_v2.nc"). We look at map-minus-data differences averaged over biomes, or over biomes and years. These biome or biome/year averages are taken only over those pixels/months that are covered by data, and with at least $400\,\mathrm{m}$ water depth to avoid coastal data (these coastal data may otherwise dominate the diagnostics as the methods do not take the special environment along the coasts into account). Spatial averages are further restricted to the valid area of each method; this may slightly favor methods with less surface coverage, because fewer data pixels are then included in the mismatch.

In addition to averaged map-data differences, we also consider time series of corresponding selective averages of the $pCO_2$ maps themselves sampled at the data locations/times.

#### 3.5.2 The relative IAV mismatch $R^{\mathrm{iav}}$

As an overall measure of the mismatch between a given mapping product and the data with respect to interannual variations in a given biome, we use the amplitude of the average difference between the map and the comparison data: (1) Averages of the map–data difference are taken over biomes and years, restricted to data-covered open-ocean pixels/months as described in Sect. 3.5.1. (2) A mismatch amplitude $M^{\mathrm{iav}}$ is calculated as the temporal standard deviation of these biome/yearly average differences over the 1992–2009 analysis period (if a method does not cover all this analysis period, statistics are calculated for a correspondingly shorter period (Table 2), despite the slight inconsistency due to IAV). (3) To be able to set these mismatch amplitudes $M^{\mathrm{iav}}$ into perspective, we similarly determine the mismatch amplitude $M^{\mathrm{iav}}_{\mathrm{benchmark}}$ of "benchmark" fields where any oceanic IAV has been removed. The benchmark maps have been created from the mean seasonal cycle of the respective original maps. As the missing $pCO_2$ increase would cause unduly large mismatches between the benchmark and the data, we added the year-to-year atmospheric $pCO_2$ increase, which is suitable as

it has negligible interannual variations compared to oceanic $p\mathrm{CO_2}$; we use the same atmospheric increase based on atmospheric $\mathrm{CO_2}$ data as used to fill invalid pixels (Sect. 3.2). (4) We then obtain a relative IAV mismatch for the given method and biome as

$$R^{\mathrm{iav}} = \frac{M^{\mathrm{iav}}}{M^{\mathrm{iav}}_{\mathrm{benchmark}}} \cdot 100\% \qquad (1)$$

It states by how much an estimate fits the data better due to its interannual variations, compared to a state of "no knowledge" about IAV. Alternatively, Eq. 1 can be seen as a normalization of the IAV mismatch to signal size: As the benchmark fields do not contain any IAV, their mismatch amplitudes $M^{\mathrm{iav}}_{\mathrm{benchmark}}$ reflect the IAV in the data (influences of variations in data density will affect $M^{\mathrm{iav}}$ and $M^{\mathrm{iav}}_{\mathrm{benchmark}}$ in similar ways). Calculating the benchmark from each product's own seasonal cycle ensures a criterion comparable between the mapping methods (though the seasonal cycles are quite similar for all methods anyway, see Sect. 4.1.1 below).

It is difficult to decide which $R^{\mathrm{iav}}$ values can be regarded as sufficient for IAV to be represented in a given map. For this paper, we present all IAV results that manage to stay below $75\%$. This is an ample threshold, but in the light of possible ambiguities in the $R^{\mathrm{iav}}$ calculation we prefer it over a stricter selection. To nevertheless make the likely range visible, we de-weight results with higher $R^{\mathrm{iav}}$ by smaller line thickness in all time series plots.

To verify that the selection criterion is not unduely biased by the fact that some methods use SOCAT data and others use LDEO data (Table 3), IAV mismatch diagnostics have also been calculated from the LDEOv2013 database (Takahashi et al., 2014a) (monthly binned), which is used as data source by some mapping methods. LDEOv2013 shares large parts of data points with SOCATv2. Mismatch values are slightly different depending on database, but qualitatively consistent.

#### 3.5.3 The relative monthly mismatch $R^{\mathrm{month}}$

An overall measure of mismatch on the monthly time scale is calculated analoguously to Sect. 3.5.2, except that monthly mismatches are used rather than yearly averaged mismatches, and that the benchmark is the year-to-year atmospheric increase without any seasonality. Thus this measure is mainly sensitive to the seasonal cycle as the largest month-to-month feature.

### 3.6 Sea–air flux calculation

Sea–air $\mathrm{CO_2}$ flux fields $f$ have been calculated from the $p\mathrm{CO_2}$ fields by

$$f = k\varrho L(p\mathrm{CO_2} - p\mathrm{CO_2^{atm}}) \qquad (2)$$

with piston velocity $k$ (employing the widely used quadratic dependence on wind speed as in Wanninkhof (1992) but scaled globally according to Naegler (2009), and reduced to 10% over ice as in Takahashi et al. (2009)), water density $\varrho$, $\mathrm{CO_2}$ solubility $L$, and atmospheric $\mathrm{CO_2}$ partial pressure $p\mathrm{CO_2^{atm}}$. The values of these auxiliary fields have been calculated from various data sets (e.g., NCEP wind speeds (Kalnay et al., 1996), OAFlux SSTs and ice cover (Yu and Weller, 2007)) as in Rödenbeck et al. (2013, see there for details) and used identically for all mapping methods, i.e., the uncertainties in the flux parameterization do not enter the comparison considered here.

As for $p\mathrm{CO_2}$, we consider the flux averaged over biomes or the global ocean. Interannual flux variations are again calculated as 12-month running means. Their amplitude $A^{\mathrm{iav}}$ is measured as temporal standard deviation of the yearly flux over the 1992–2009 analysis period. From the amplitudes $A^{\mathrm{iav}}_i$ of the individual mapping methods, we calculate an ensemble mean inversely weighted by the relative IAV mismatches $R^{\mathrm{iav}}_i$ (for methods with $R^{\mathrm{iav}}_i < 75\%$)

$$\overline{A^{\mathrm{iav}}} = \frac{\sum_{i=1}^{n} A^{\mathrm{iav}}_i / R^{\mathrm{iav}}_i}{\sum_{i=1}^{n} 1/R^{\mathrm{iav}}_i} \qquad (3)$$

Methods not covering the full analysis period are discarded in this average as there would be significant spurious changes in the amplitude if any of the El Niño anomalies in 1992 or 1997 was not included.

## 4 Results and Discussion

We first provide an overview on the estimated seasonal and interannual variations in oceanic biomes (Sect. 4.1), and the ability to estimate them from $p\mathrm{CO_2}$ data and available mapping methods. We then discuss interannual variations in the sea–air $\mathrm{CO_2}$ flux in more detail (Sect. 4.2).

### 4.1 Biome-average $p\mathrm{CO_2}$ time series

#### 4.1.1 Seasonality

As introductory example, we first consider surface ocean $p\mathrm{CO_2}$ averaged over the North Atlantic Subtropical Permanently Stratified biome, which belongs to the relatively well observed regions and shows a pronounced seasonal cycle in $p\mathrm{CO_2}$ (Schuster et al., 2013). Fig. 3 panel (a) shows monthly $p\mathrm{CO_2}$ time series from the whole ensemble. For clarity of details, three arbitrary years have been selected. The results of the mapping methods generally agree with each other in terms of the mean and the seasonal cycle to within about $10\,\mu\mathrm{atm}$.

Panel (b) compares the mapping results to the SOCATv2 monthly gridded observations. To this end, mapping results have been averaged only over those locations/times where SOCATv2 comparison data exist. As these are the locations/times where (most of) the estimates are directly constrained, the mapping results generally follow the data

closely, and the ensemble spread is often smaller than in panel (a). In some months (e.g., Sept. 2003 or July 2004) these selective averages deviate considerably from the whole-biome average, likely reflecting spatial sampling biases in the presence of spatial $pCO_2$ gradients. In such months, the ensemble spread tends to be higher than in months less affected by sampling biases.

To objectively compare our results to the in-situ data, we calculate the average difference between the mapped $pCO_2$ (at the data location) and the SOCATv2 monthly gridded values (panel (c)). In general, differences of the monthly values lie within about $\pm 10\,\mu\mathrm{atm}$. *NIES-OTTM* deviates farther, likely because this approach is strongly determined by the modelled seasonal cycle and thus does not follow the data more closely.

Time series for the complete set of biomes are given in the Appendix. In terms of seasonality, the mapping methods show similar phasing and amplitude in almost all extratropical biomes (Fig. A1), with few exceptions mainly in the North Atlantic Subpolar Seasonally Stratified biome and the Southern Ocean. The spread in the North Atlantic is somewhat surprising given the relatively good data coverage. Possibly, this area has larger spatial heterogeneity not adequately represented by (some of) the methods. *NIES-OTTM* shows a seasonal cycle opposite to the other methods, a behaviour present in many biogeochemical process models in high latitudes (Valsala and Maksyutov, 2010; Schuster et al., 2013). Methods agree on smaller seasonal amplitude in the tropics, though substantial differences in amplitude and phase exist.

#### 4.1.2 Interannual variability (East Pacific Equatorial biome)

Interannual variability is exemplified with the East Pacific Equatorial biome, which is also relatively well observed, and features large coherent interannual variations in $pCO_2$ associated with the ENSO cycle (e.g., Feely et al., 1999). Fig. 4 panel (a) shows the results of those mapping methods with IAV mismatches ($R^{\mathrm{iav}}$, Sect. 3.5) of at most $75\%$ of signal size. This selection has been done because interannual signals in the data turn out not to be represented in all mapping methods; thus the full ensemble (Appendix Fig. A2 panel "Biome 6") would highly overestimate the uncertainty of IAV. All the 8 selected mapping methods consistently show a reduction in ocean surface $pCO_2$ during El Niño conditions (1987, 1992, strong El Niño 1997/98, weak El Niño's also 2002, 2006, 2009/10), though partially with different amplitudes (see Sect. 4.2.1 for the particularly low amplitude of *UEA-SI*). Methods regressing $pCO_2$ against external drivers (*JMA-MLR*, *UNSW-SOMLO*, *NIES-SOM*, *ETH-SOMFFN*) tend to show mutually similar time variations also on the finer 1–2 year time scale (e.g., 2008–2009), while statistical interpolation methods (*UEA-SI*, *Jena-MLS*) may show different finer-scale features. Despite this biome-wide difference, averages at data-constrained pixels only (Fig. 4 panel (b)) mostly are much more consistent between methods. This is expected as this selective average excludes all the gap-filled pixels where values naturally depend much more on the applied mapping method. Most strikingly, in the data-poor periods up to 1988, regression and interpolation methods (as far as they cover these periods) strongly differ in the whole-biome average (panel (a)), while they more closely agree at the data-covered pixels (panel (b)). This illustrates that the statistical interpolation methods solely rely on the $pCO_2$ data constraint while regression methods bridge data gaps as their variability originates from the driver data that are available throughout time. In the more data-rich periods (since about 1992 in this biome), interpolation and regression methods do agree in many features even in the whole-biome average (panel (a)). Due to the complementary origin of the variability in these method classes (Fig. 1), this agreement confirms that, at least in this biome, (1) sufficient interannual information is contained in the available $pCO_2$ observations (in the more densely sampled period), and (2) the signals provided through the driver data of the regression methods largely capture the essential modes of interannual $pCO_2$ variability.

Note that the selective average over data-covered pixels (panel (b)) also leads to temporal features very different from the full average (e.g., the peak in 2001), revealing sampling biases that alias seasonal variations and spatial gradients into the yearly/spatial average due to not fully representative sampling. These sampling biases pose the most prominent challenge to all the mapping methods.

Panel (c) shows the biome/yearly average difference between the interpolated $pCO_2$ fields and the SOCATv2 monthly gridded data set (Sect. 3.5), reflecting the mismatch of mean, trend, and interannual variations (the sampling biases mentioned before should largely cancel out in this difference). Most mapping methods have a temporal mean mismatch (bias) of less than a few $\mu\mathrm{atm}$. The year-to-year mismatches are of different magnitudes for the individual mapping methods (note that the larger mismatches in 2009/2010 occur in a period of very few data points and may not be representative). Though the estimated interannual features can only be trusted if the year-to-year mismatches are small (necessary condition), small year-to-year mismatches are not yet a sufficient condition for correct interannual variations: Even if the available data points are fit well, the extrapolation to data-void areas can be wrong ("over-fitting", see more discussion in Sect. 4.2 below). Therefore, we stress that the mismatch amplitudes are not meant to represent a detailed ranking of quality of the methods. Nevertheless, we take it as an encouraging finding that mapping methods with smaller IAV mismatch (e.g., passing the more strict relative IAV mismatch criterion of $R^{\mathrm{iav}} < 30\%$ [*Jena-MLS*, *ETH-SOMFFN*]) are also closer to each other in the whole-biome average (panel (a)). Even this stricter selection comprises methods regressing or not regressing $pCO_2$ against external drivers, i.e., complementary ways of extrapolating to data-void ar-

eas/periods (Fig. 1, Table 3 table footnote $e$). This reinforces conclusions (1) and (2) above and confirms that meaningful interannual estimates can be achieved from the available $p\mathrm{CO_2}$ data and mapping methods in the Equatorial Pacific.

#### 4.1.3 Interannual variability (other biomes)

All mapping methods agree that the East Pacific Equatorial biome considered before (Sect. 4.1.2) has the largest interannual variability of all biomes (Fig. A2). The other biomes have much less interannual variability, leaving the rising trend (similar to the atmospheric $\mathrm{CO_2}$ increase) as the most prominent interannual feature. There is one mapping method (*NIES-OTTM*) without a trend, a feature not however supported by the data (see large data mismatch with systematic trend in Fig. A3). Except for the West and East Pacific Equatorial biomes, the small year-to-year variations around the rising trend are not generally consistent between the mapping methods (ensemble spread similar or larger than the variations themselves).

Overall, mean mismatches (biases) are on the order of $3$–$4\,\mu\mathrm{atm}$ in all biomes (Fig. A3). As the mismatches do not consistently rise or fall over time, they confirm the estimated $p\mathrm{CO_2}$ trends (except for *NIES-OTTM* that does not have the rising trend in $p\mathrm{CO_2}$). The year-to-year mismatches have amplitudes of $3$–$4\,\mu\mathrm{atm}$ in some methods, but also mismatches as large or larger than the interannual variations for other methods ($R^{\mathrm{iav}} > 75\%$, dashed lines). Except for the North Atlantic Subtropical Seasonally Stratified biome, each ocean region has at least some mapping methods with relative IAV mismatch below $60\%$ or even $30\%$, including both interpolation methods as well as linear and non-linear regressions. Methods tying IAV to process model simulations (*PU-MCMC*, *NIES-OTTM*) often have large relative IAV mismatches, except for *PU-MCMC* in the Northern Pacific biomes.

### 4.2 Sea–air $\mathrm{CO_2}$ flux variability

In order to link the estimated $p\mathrm{CO_2}$ variability to variability of sea–air $\mathrm{CO_2}$ exchange as considered for the Global Carbon Project (GCP) (Le Quéré et al., 2015), we calculated sea–air $\mathrm{CO_2}$ fluxes $f$, using the same gas exchange formulation for each mapping method (Sect. 3.6).

#### 4.2.1 The East Pacific Equatorial biome

We first consider again the East Pacific Equatorial biome identified above as the biome with the largest interannual variability. Fig. 5 panel (a) provides its sea–air $\mathrm{CO_2}$ fluxes estimated by 8 selected mapping methods (having relative IAV mismatch $R^{\mathrm{iav}} < 75\%$ for biome-averaged $p\mathrm{CO_2}$). The year-to-year flux variations are mainly driven by the $p\mathrm{CO_2}$ variability (compare to Fig. 4 panel (a)). Again, interannual features are largely similar between the mapping methods in this biome, but differ in their amplitudes (Fig. 5 panel (b)). There is some tendency that the mapping methods with smaller IAV mismatch show larger interannual amplitudes. Strikingly low interannual variability is found in *UEA-SI*, while fitting the data with $R^{\mathrm{iav}} = 52\%$ better than various other methods. This method moves away from the estimated mean seasonality only in the close vicinity of the data points, as justified by the short auto-correlation lengths of near-simultaneous $p\mathrm{CO_2}$ levels found in the $p\mathrm{CO_2}$ data (Jones et al., 2012). It thus gives a lower bound of IAV secured by the data information (Jones et al., 2015). As interannual features can be assumed to be more spatially coherent than features on the time scale of ship cruises (especially in the Equatorial Pacific), the low IAV amplitudes by *UEA-SI* are likely an underestimate.

#### 4.2.2 The global ocean

Fig. 5 panel (c) provides global sea–air $\mathrm{CO_2}$ fluxes estimated by 10 selected mapping methods (having relative IAV mismatch $R^{\mathrm{iav}} < 75\%$ for global $p\mathrm{CO_2}$). These mapping methods mostly agree in their decadal variations, with a pronounced decadal enhancement in ocean $\mathrm{CO_2}$ uptake after the year 2000, preceded by a period of little decadal change or rather weakening uptake (see Fig. A7). This confirms a feature also simulated by process models (see Fig. 7 of Le Quéré et al. (2015) and discussion in Sect. 3.6 of Rödenbeck et al. (2014)). One of the areas contributing to this change in decadal trends is the Southern Ocean, where Landschützer et al. (2015) found consistency of decadal trends between *ETH-SOMFFN* and *Jena-MLS* having relatively low $R^{\mathrm{iav}}$ values there.

There is less agreement in the sub-decadal variations of the global sea–air $\mathrm{CO_2}$ flux, despite the much closer mutual agreement of the same mapping methods in the well-constrained East Pacific Equatorial biome (Fig. 5 panel (a)). This lower agreement reflects the more uncertain flux contributions from the poorly data-constrained areas. For example, the larger sub-decadal variations by *Jena-MLS* to large part originate from the South Pacific Subtropical Permanently Stratified biome (Fig. A4 panel "Biome 7"), which is a data-poor region and therefore may recieve spurious variability from the Equatorial Pacific extrapolated too far south (indeed, the amplitude of the variations reduces with shorter latitudinal extrapolation radius (latitudinal a-priori correlation length, Sect. 3.3 of Rödenbeck et al., 2014)), though according to the $R^{\mathrm{iav}}$ criterion these larger variations match the data better than the smaller variations. Another contributor of sub-decadal *Jena-MLS* variability is the Pacific sector of Biome 16: In the Southern Ocean, essentially only two areas (South of New Zealand and South-West of Patagonia, respectively) are data-covered for multiple years, such that signals from there are extrapolated into their data-void surroundings. Due to this low data coverage, the Southern Ocean biomes 15 and 16 also contribute considerably to the ensemble spread in general (Fig. A4). Unforunately, the absence of data also

means that we cannot validate or falsify the different extrapolations. In summary, despite the success in constraining $CO_2$ fluxes in the Equatorial Pacific from available data and mapping methods (Sect. 4.2.1), estimates of year-to-year variations in the global sea–air $CO_2$ flux face larger uncertainties due to the undersampled regions.

Despite these differences in the detailed variations, the amplitude of global flux IAV (Sect. 3.6) is relatively consistent (panel (d)). The global weighted ensemble mean $\overline{A^{\mathrm{iav}}}$ (Eq. 3) is $0.31\,\mathrm{PgC\,yr^{-1}}$ (horizontal line in panel (d)). Many biogeochemical process models have less variability than that (mean of $0.20\,\mathrm{PgC\,yr^{-1}}$ in Le Quéré et al. (2015)) and thus likely underestimate IAV in the ocean carbon sink (compare Séférian et al., 2014; Turi et al., 2014). Inverse estimates based on atmospheric $CO_2$ data show both larger and smaller oceanic IAV (Peylin et al., 2013), reflecting that they can constrain land variability but less so ocean variability.

Though the primary strength of the $pCO_2$ constraint lies in its information on temporal variations and smaller-scale spatial variations, we also consider the long-term mean global sea–air $CO_2$ exchange. The total mean flux (comprising both uptake induced by anthropogenic atmospheric $CO_2$ rise and natural river-induced outgassing) estimated by the different methods ranges between $-1.36\,\mathrm{PgC\,yr^{-1}}$ and $-1.96\,\mathrm{PgC\,yr^{-1}}$ (for the 1992–2009 analysis period), with a weighted ensemble mean (analogous to Eq. 3 but using the inverse mean $pCO_2$ bias as weights) of $-1.75\,\mathrm{PgC\,yr^{-1}}$. This is consistent within uncertainties with the independent estimate from inverting ocean-interior carbon data of $-1.7\,\mathrm{PgC\,yr^{-1}}$ (Gruber et al., 2009) nominally for 1995. Subtracting a river-carbon induced outgassing flux of $0.45\,\mathrm{PgC\,yr^{-1}}$ (Jacobson et al., 2007), the ensemble mean corresponds to an anthropogenic $CO_2$ uptake of $-2.2\,\mathrm{PgC\,yr^{-1}}$. This is again consistent within uncertainties with the estimate from the globally integrative constraint by the atmospheric $O_2$ and $CO_2$ trends of $-2.2 \pm 0.6\,\mathrm{PgC\,yr^{-1}}$ given by Manning and Keeling (2006) for the slightly different 1993–2003 period.

## 5 Conclusions

Measurements of surface-ocean $pCO_2$, mapped into continuous space-time fields, offer a much more direct way to quantify sea–air $CO_2$ fluxes and their variations than previously available approaches (model simulations, atmospheric inversions, ocean-interior inversions). Taking advantage of an ensemble of 14 partially complementary surface-ocean $pCO_2$ mapping methods recently collated by the SOCOM initiative, we analysed sea–air $CO_2$ flux variability globally and for a subdivision of the ocean into 17 biomes (Fay and McKinley, 2014). This study has found that:

- Surface-ocean $pCO_2$ data together with mapping methods constrain the seasonality of regional $pCO_2$ essentially in all ocean biomes (mostly within $10\,\mu\mathrm{atm}$).
- Interannual variations of regional $pCO_2$ are constrained at least in the more densely observed ocean regions (tropical Pacific, parts of the Northern temperate Pacific and Atlantic). The tropical Pacific is consistently estimated as the biome with the largest interannual variations, with reduced $CO_2$ uptake during El Niño periods. The global ocean $CO_2$ uptake is estimated to have gradually increased since about 2000, with little decadal change prior to that.
- Interannual variations in the global sea–air $CO_2$ flux are estimated to have an amplitude of $0.31\,\mathrm{PgC\,yr^{-1}}$ (average across mapping methods weighted according to IAV mismatch). Therefore most biogeochemical process models appear to significantly underestimate this variability (Le Quéré et al., 2015, quote a model-derived amplitude variation of $0.2\,\mathrm{PgC\,yr^{-1}}$).
- Though the primary strength of the $pCO_2$ constraint lies in its information on temporal variations and smaller-scale spatial variations, the estimated net integrated global sea–air $CO_2$ flux of $-1.75\,\mathrm{PgC\,yr^{-1}}$ (weighted ensemble mean) is consistent within uncertainties with the independent estimates based on inverting ocean-interior carbon data and on atmospheric $O_2$ and $CO_2$ trends.

For forthcoming analyses involving data-based sea–air $CO_2$ flux products, we recommend –if possible– to use several interpolation products, or at least to test the robustness of the features under consideration by checking the consistency between several products. In particular, agreement between complementary mapping methods taking variability either from driver data or directly from $pCO_2$ data (Fig. 1), as found here for the interannual variations in the tropical Pacific, lends great support to the estimated features, as it shows consistency between different information sources.

However, the mapping products should carefully be selected and weighted according to suitable performance diagnostics, to ensure their suitability in a given purpose. The presented "relative IAV mismatch" criterion provides a necessary condition for IAV applications. Analoguous "relative mismatch" criteria can also be defined and calculated for other time scales. However, as discussed in the paper, it would be even better to use sufficient conditions (e.g., derived by testing the power of the mapping methods to reconstruct modelled $pCO_2$ fields from pseudo data subsampled as the real data). Such sufficient conditions are not yet available for the SOCOM ensemble, but are planned in forthcoming studies.

SOCOM does not identify an "optimal" mapping method or method class. We also discourage any ensemble averaging (or medians, etc.) of full spatio-temporal fields or time series, as this would result in variations that are not self-consistent any more and fit the data less well than individual products. Only for scalar statistical quantities of the spatio-

temporal fields, such as amplitudes of variation, correlation coefficients, etc., it may make sense to summarize the ensemble into averages of these quantities, weighted according to the above-mentioned performance diagnostics.

Many of the $pCO_2$ mapping products are updated when new data sets become available, and the mapping methods are subject to further development. The SOCOM intercomparison may serve to stimulate such developments, though results should not be assessed in terms of their position in the ensemble, but only in terms of objective criteria. At the website http://www.bgc-jena.mpg.de/SOCOM/ we aim to provide an updated list of products and ensemble analyses. SOCOM welcomes further members contributing estimates of the spatio-temporal $pCO_2$ field or the sea–air $CO_2$ flux based on surface-ocean carbon data.

The basis of all mapping products considered here are extensive $pCO_2$ observations over many years. Even when external information is used to bridge data gaps (Fig. 1), a minimum amount of data in time or within areas of similar biogeochemical behaviour is indispensible. Missing data may not only lead to miss out existing features, but even to create spurious features due to sampling biases. Though the exact limits to interpolation capacity can only be determined through targeted studies (e.g., by running interpolation schemes only on part of the data and then comparing to the other part), this study already shows that (1) with realistic sampling efforts (e.g. in the above-mentioned well-constrained regions) and available mapping methods, constraining $pCO_2$ variability is possible (as in Fig. 5a, Sect. 4.2.1), but (2) undersampled regions limit our current ability to determine the global total flux in its finer detail (Fig. 5c, Sect. 4.2.2). This highlights the high priority that should be given to sustaining the ongoing sampling and to closing observational gaps. As many of the undersampled regions are not well accessible by ships, autonomous sampling devices, such as BioARGO floats (Claustre et al., 2010), seem indispensible as additional observation component. In addition to the actual measurements, the use of $pCO_2$ observations in regional and global sea–air $CO_2$ flux products also depends on the continuation of all the efforts to quality-control the data and to provide them in a consistent and user-friendly form.

## Appendix A

### A1 *"UEA-SI"* (Statistical interpolation)

*Method description:* The approach combines temporal interpolation through curve fitting (1–4 seasonal harmonics and a linear trend) (Masarie and Tans, 1995; Schuster et al., 2009) and spatial interpolation using the concept of spatial de-correlation lengths, or a 'radius of influence', interpolating data based on the likely similarity between spatially separated points (Cressman, 1959; Levitus, 1982). In addition, cubic spline fitting is used to move away from the fitted mean seasonal cycle to incorporate interannual variations where data points exist. The de-correlation scales applied in the interpolation are determined from the auto-correlation characteristics of the $pCO_2$ data along ship-tracks or in time (Jones et al., 2012).

*Main intention / focus:* To produce a $pCO_2$ data set for various uses. To quantify the impact of modes of climate variability on $pCO_2$ and air-sea fluxes. The chosen approach departs from other methods through its purely statistical approach; it does not use any other data sources than $pCO_2$.

*Documentation:* Jones et al. (2015)

*Contact:* Steve Jones.

### A2 *"OceanFlux-SI"* (ESA STSE OceanFlux Greenhouse Gases)

*Method description:* The in-situ $pCO_2$ data within SOCAT are first corrected to a common satellite derived temperature dataset using an isochemical temperature dependence. This creates an in-situ dataset with a common SST reference. Each in-situ datapoint is then corrected to the year 2010 by assuming a trend of $1.5\,\mu\mathrm{atm\,yr^{-1}}$. The data are then binned into a monthly 1x1 degree format. These monthly binned data are kriged to produce a spatially complete dataset (Goddijn-Murphy et al., 2015). We finally generate an interannual time series by (1) cyclically using this climatological dataset over time, (2) adding a prescribed trend of $1.5\,\mu\mathrm{atm\,yr^{-1}}$ in $pCO_2$, and (3) correcting the $pCO_2$ values according to the difference between the climatological SST and the actual satellite-derived SST at each time and location (Shutler et al., in revision). We use here the original dataset (not filtered based on the uncertainty).

*Main intention / focus:* Produce a spatially complete monthly climatology of $pCO_2$ data for 2010 that uses a consistent temperature dataset which is valid at a consistent depth in the water.

*Documentation:* Goddijn-Murphy et al. (2015) (monthly climatology), Shutler et al. (in revision) (interannual variations).

*Contact:* Jamie Shutler

### A3 *"Jena-MLS"* (Data-driven mixed-layer scheme)

*Method description:* The mixed-layer scheme is a data-driven interpolation scheme, primarily based on $pCO_2$ observations but also compatible with the dynamics of mixed-layer carbon content. Firstly, the sea–air $CO_2$ fluxes and the $pCO_2$ field are linked to the spatio-temporal field of ocean-internal carbon sources/sinks through parametrizations of sea–air gas exchange, solubility, and carbonate chemistry, as well as a budget equation for mixed-layer Dissolved Inorganic Carbon (DIC). Then, the ocean-internal carbon sources/sinks are adjusted to optimally fit the $pCO_2$ field to the $pCO_2$

observations (in the present version oc_v1.3: SOCATv3, Bakker et al., in preparation). Spatio-temporal interpolation is achieved by Bayesian a-priori smoothness constraints with prescribed spatial and temporal de-correlation scales; temporal interpolation also results from the inherent relaxation time scales of the mixed-layer carbon budget. Though the process parametrizations are driven by SST, wind speed, mixed-layer depth (MLD) climatology, alkalinity climatology, and some auxiliary variables, this external variability only determines features not constrained by the $pCO_2$ observations (e.g., day-to-day variations, or variability in data-void areas/periods), while the estimated $pCO_2$ field in well-constrained areas/periods is only determined by the observed signals (no regression against drivers).

*Main intention / focus:* Global $CO_2$ flux field product primarily based on observations only, with a focus on flux variability, also to be applied as ocean prior in atmospheric $CO_2$ inversion (in particular the Jena inversion, Rödenbeck (2005)). The mixed-layer scheme has been chosen because it can be extended to link carbon variability to further observables (mixed-layer $PO_4$, atmospheric $O_2$), for using these as additional independent data constraints.

*Documentation:* Rödenbeck et al. (2013) (method description and seasonality); Rödenbeck et al. (2014) (interannual variations and link to oxygen).

*Contact:* Christian Rödenbeck

### A4 *"CU-SCSE"* (Surface Carbon State Estimation)

*Method description:* The Surface Carbon State Estimate (SCSE v1.0, Jacobson et al. (in preparation)) is a Kalman filter interpolation scheme for mapping $pCO_2$ over the global ocean during the entire period for which SOCAT point observations are available. It is designed to provide a statistically well-characterized prior estimate to an atmospheric $CO_2$ analysis like CarbonTracker. SCSE tracks the time-varying magnitudes of a set of basis functions, determined as an optimal difference from a reference state composed of the Takahashi et al. (2009) $pCO_2$ climatology for year 2000 plus a $1.5\,\mu\mathrm{atm\,yr^{-1}}$ global trend. Uncertainties are explicitly characterized by a full-rank posterior covariance matrix, which can then be used to produce realistic error estimates for arbitrary spatial domains. SCSE is a gridded estimation scheme that tracks $pCO_2$ for each $1^\circ \times 1^\circ$ grid cell, but its effective spatial resolution is controlled by the number of basis functions used within each of 10 defined ocean basins. The number of basis functions used within each basin varies with time and is determined by the number of available observations. This is intended to allow higher resolution at times and places where there are more $pCO_2$ measurements. The basis functions include empirical orthogonal functions (EOFs) of $pCO_2$ from a set of CMIP5 ocean carbon cycle simulations, intended to represent the within- and across-model variations of climatology, trends, and variability on inter-annual to decadal time scales. They are assigned widely different relaxation time scales (3 months – 5 years) as determined by the EOF analysis.

*Main intention / focus:*

*Documentation:* Jacobson et al. (in preparation)

*Contact:* Andy Jacobson

### A5 *"AOML-EMP"* (Diagnostic model using empirical relationships)

*Method description: AOML-EMP* uses empirical relationships between surface-ocean $pCO_2$ and SST, trained based on sub-annual variations in the Takahashi $pCO_2$ climatology and the associated climatological SST values. These relationships are then applied to interannually varying SST (using the NOAA optimal interpolation SST product www.ncdc.noaa.gov/oisst). The original analysis of Park et al. (2010a) does not implicitly include the effect of rising atmospheric $CO_2$ levels. In the modified Park et al. analysis presented in Le Quéré et al. (2015) the effect of increasing atmospheric $CO_2$ on the surface ocean is simulated by applying the output of the "$CO_2$-only" run of NCAR CCSM-3 model (National Center for Atmospheric Research's Community Climate System Model Version 3) to each grid cell over the time period. The sub-decadal variability is the same for each approach as they are based on the same $pCO_2$ mapping. The decadal trend of $CO_2$ flux calculated from the original *AOML-EMP* approach shows a slight decrease in uptake while the modified approach shows an increase in uptake that is attributed to a negative feedback in $CO_2$ uptake due to ocean warming that is overwhelmed by increased anthropogenic $CO_2$ uptake.

*Main intention / focus:* Data-driven global $CO_2$ flux product

*Documentation:* Park et al. (2010a,b)

*Contact:* Geun-Ha Park

### A6 *"UEx-MLR"*

*Method description:* Multi-parameter regression in 12 separate ocean regions (RECCAP regions, see http://www.globalcarbonproject.org/global/pdf/RECCAP_Soft_%20Protocol.v4.pdf and Fig. 1 in Schuster et al. (2013)) from 1990 to 2012. Main data stream used as constraint: SOCATv2 gridded product (Sabine et al., 2013) plus additional recent gridded data (all on 1 degree latitude by 1 degree longitude by 1 month). Driver variables used: SST, Mixed layer depth, chlorophyll-a, atmospheric $pCO_2$.

*Main intention / focus:* Seasonal through interannual variability of the sea–air $CO_2$ flux.

*Documentation:* Schuster et al. (2013) (RECCAP)

*Contact:* Ute Schuster

### A7 *"JMA-MLR"*

*Method description:* The global ocean was divided into 44 sub-regions based on the features of observed $pCO_2$ and

SST/SSS/Chl-a variability and then optimal equations for estimating $pCO_2$ in the sub-regions were derived from multiple regressions using SST, SSS and Chl-a as independent variables. Rather than using time as independent variable, secular trends of $pCO_2$ (for wider biomes than the sub-regions) were evaluated separately from multiple regressions, subtracted from the data, and re-added to the $pCO_2$ map. Observed $pCO_2$, SST and SSS in SOCATv2 and satellite Chl-a (SeaWiFS and MODIS/Aqua: http://oceancolor.gsfc.nasa.gov; before 1997, the climatology of satellite Chlorophyll-a data are used) are used to derive equations and analytical SST (MGDSST: Kurihara et al. (2006)), SSS (MOVE/MRI.COM-G: Usui et al. (2006)) and the same Chl-a data mentioned above are used to reconstruct the $pCO_2$ fields.

*Main intention / focus:* To map global $pCO_2$ and $CO_2$ flux field based on surface observation data and evaluate the interannual variability and long-term trend of global ocean $CO_2$ uptake. The merits of using simple multiple regression analysis for estimating $pCO_2$ include its possibility to give oceanographic explanations for the $pCO_2$ variability.

*Documentation:* Iida et al. (2015) (method description and trend analysis)

*Contact:* Yosuke Iida

### A8 *"UNSW-SOMLO"* (Self-Organizing Multiple-Linear Output)

*Method description:* In this approach we couple a neural network clustering algorithm with a multiple linear regression (MLR) to diagnose monthly ocean surface $pCO_2$ distributions from 1998 through to 2011. The algorithm first captures larger-scale ocean dynamics by a data-based clustering of the grid cells into "biogeochemical fingerprints" using a self-organizing map (SOM). The SOM approach utilizes the SOCATv2 gridded $pCO_2$ product along with co-located SST, SSS, Chl-a, MLD, and geographical information (n-vector) to iteratively cluster the dataset into a set of 196 neurons (the spatial domains of which we refer to as biogeochemical fingerprints). Within each neuron, MLRs are then derived between $pCO_2$ and the optimal set of sea-surface temperature/salinity/Chl-a, MLD, and atmospheric $xCO_2$. Thus, each MLR can be thought of as a local-scale optimizer that follows the global non-linear optimization analysis performed by the SOM. To predict $pCO_2$ using any independent set of driver data, a similarity measure is first used to determine which neuron best represents the driver data values, then the $pCO_2$ value is predicted using the regression parameters established with training data of that neuron. We call this approach SOMLO: self-organizing multiple linear output.

*Main intention / focus:* To diagnose monthly ocean surface $pCO_2$ distributions and air-sea $CO_2$ fluxes from 1998 through to 2011, and to advance our understanding of seasonal to inter-annual variability.

*Documentation:* Sasse et al. (2013)

*Contact:* Tristan Sasse

### A9 *"ETH-SOMFFN"* (A Combined 2-Step Neural Network approach)

*Method description:* As a first step, a self-organizing map (based on climatological $pCO_2$, SST, SSS, MLD, and Chl-a) is used to cluster the global ocean into biogeochemical provinces. Within each province, a feed-forward network is then used to reconstruct the non-linear relationship between drivers (SST, SSS, MLD, Chl-a [before 1998 using a climatology], and atmospheric $xCO_2$) and gridded $pCO_2$ observations from SOCAT.

*Main intention / focus:* Produce global $pCO_2$ and $CO_2$ flux maps; investigate seasonal and inter-annual variability within the study period

*Documentation:* Landschützer et al. (2013, 2014)

*Contact:* Peter Landschützer

### A10 *"CARBONES-NN"*

*Method description: CARBONES-NN* is a neural network framework developed within the EU-FP7 project CARBONES (http://www.carbones.eu/wcmqs/) that maps surface ocean $pCO_2$ observations to first-order explanatory variables. As explanatory variables, it uses observations from satellites (Surface Chlorophyll climatology from SeaWiFS), model outputs (SST, SSS, MLD) from the MERCATOR ocean reanalysis, previous step $pCO_2$ estimates (recursive approach) and latitude as a proxy for atmospheric conditions. A two-step neural network approach is applied based on a Multi Layer Perceptron network coupled with a variational data assimilation scheme. A first calibration step adjusts the seasonal component of $pCO_2$ using climatological data (reference year 2000; from Takahashi et al. (2009) sampled at the points where there are measurements). This step recreates a 2D monthly climatology of $pCO_2$ that is similar to the one of Takahashi et al. (2009), but also different as the interpolation is based on the explanatory variables. A second step uses the raw $pCO_2$ data (LDEOv1.0, Takahashi et al. (2007)) to adjust the interannual variability of $pCO_2$ over the period 1989 to 2009. A moving assimilation window is used. Input variables and $pCO_2$ data were previously gridded at monthly temporal and $2^\circ \times 2^\circ$ spatial resolutions. Note that most of the coastal ocean $pCO_2$ data have been filtered out.

*Main intention / focus:* Produce global $CO_2$ sea–air flux maps over the past decades to be coupled in the Carbon Cycle Data Assimilation System developed at LSCE within the CARBONES project.

*Documentation:* CARBONES web site (http://www.carbones.eu/wcmqs/) and article under preparation.

*Contact:* Philippe Peylin

### A11 *"NIES-SOM"*

*Method description:* Self-organizing map with linear increasing trend with time.

*Main intention / focus:* $pCO_2$ mapping and evaluating seasonal/interannual air-sea $CO_2$ exchange.

*Documentation:* Nakaoka et al. (2013) (for North Pacific); Nakaoka et al. (in prep.) (for Pacific)

*Contact:* Shin-ichiro Nakaoka

### A12 *"NIES-NN"* (feed-forward neural network)

*Method description:* We first estimated the global trend of $pCO_2$ using the method of Zeng et al. (2014) and used this trend to normalize the $pCO_2$ data to the reference year 2000. We then modelled the spatial and seasonal variations in the reference year using a feed-forward neural network (Zeng et al., 2015b). The driver variables include SST, SSS, Chl-a, latitude, longitude, and month. For training, climatologies of the driver data are used. For prediction, we use time variant SST (it would be ideal to use time variant SSS and Chl-a as well but no such data are available in certain modeled periods). Due to the use of climatologies of the driver data and the normalized $pCO_2$ to train the neural network, the predicted $pCO_2$ does not yet contain a trend; therefore, the trend estimated in the first step is re-added to the network output. We use all data from SOCATv2 that fulfill the selection criteria elevation $< -500\mathrm{m}$, ice cover $< 50\%$, SSS $> 25$, and SST $> -10°\mathrm{C}$. Software implementation details of the model can be found in Zeng et al. (2015a).

*Main intention / focus:* Monthly $CO_2$ maps and long-term global trend.

*Documentation:* Zeng et al. (2014) (for climatology); (Zeng et al., 2015b) (for time-varying fields); Zeng et al. (2015a) (software implementation); data set doi:10.1594/PANGAEA.834398

*Contact:* Jiye Zeng

### A13 *"PU-MCMC"*

*Method description:* The Princeton $pCO_2$ product is calculated by a Bayesian inversion (using a Markov Chain Monte Carlo (MCMC) minimization algorithm) as described in Majkut et al. (2014). The $pCO_2$ field is decomposed into (A) the decadal trend, (B) the June 1995 mean value, (C) the seasonal cycle, and (D) the interannual variability. Each of these terms is derived from process model simulations, and then scaled as to optimally fit the $pCO_2$ observations. The data product that is inverted is LDEOv2010 (Takahashi et al., 2012). Two forward models were used to derive the prior fields, with the main model being GFDL's MOM4p1-BLING. For MOM4p1-BLING the underlying physical model is GFDL's Modular Ocean Model version 4.1 (Griffies et al., 2004) with three degree horizontal resolution. The biogeochemical model is Biology Light Nutrient and Gas (BLING) (Galbraith et al., 2011). The model was forced at the surface with several reanalysis products, including CORE-II (Large and Yeager, 2009), ERA-40 (Uppala et al., 2005), and NCEP-1 (Kalnay et al., 1996). Additionally, the two simulations with NEMO-PISCES from the study of Rodgers et al. (2014) were included in the analysis.

*Main intention / focus:* Seasonal through decadal variability in $pCO_2$ and air-sea $CO_2$ fluxes

*Documentation:* Majkut et al. (2014)

*Contact:* Keith Rodgers

### A14 *"NIES-OTTM"* (Ocean Tracer Transport Model with variational assimilation of surface ocean $pCO_2$)

*Method description:* The offline OTTM is run with physical data from GFDL coupled ocean-atmospheric re-analysis version-2 data for the period of 1980-2010 (Delworth et al., 2006; Gnanadesikan et al., 2006). The necessary input data used from the re-analysis are as follows: The time dependent 3-D currents, hydrography and surface 2-D variables such as MLD, heat fluxes, water fluxes and sea surface height. The physical part of OTTM calculates the evolution of tracers in the global ocean (Valsala et al., 2008). The biological model is adapted from McKinley et al. (2004). The export production in the surface euphotic zone ($0$–$140\,\mathrm{m}$) is calculated using prescribed monthly climatological phosphate and light, scaled by a spatially varying '$\alpha$' parameter which accounts for maximum export rate and for those processes which are not accounted for by the phosphate and light limitation model. The surface ocean chemistry model is taken from OCMIP-II abiotic model (Orr et al., 1999). The physical-biogeochemical model is used to simulate the surface ocean $pCO_2$ and air-sea $CO_2$ fluxes. The surface ocean $pCO_2$ in the model is constrained by a variational assimilation method in which a conservative adjoint of data-model misfit of $pCO_2$ (using the $pCO_2$ climatology and LDEOv1.0 point data (Takahashi et al., 2007)) is tracked backward in time in the 3-D ocean over an iteration window of 2 months. At each iteration, the forward model corrects the initial and boundary condition of DIC (Dissolved Inorganic Carbon) according to the weighted adjoints. The iterations are truncated when the mismatch falls below a minimum value of $10\,\%$ of its initial value (see Valsala and Maksyutov, 2010).

*Documentation:* Valsala and Maksyutov (2010)

*Contact:* Vinu Valsala

*Acknowledgements.* We would like to thank all colleagues and funding agencies involved in the collection, quality control, and synthetization of $pCO_2$ data, which are the basis of all mapping products. The Surface Ocean $CO_2$ Atlas (SOCAT) is an international effort, supported by the International Ocean Carbon Coordination Project (IOCCP), the Surface Ocean Lower Atmosphere Study (SOLAS), and the Integrated Marine Biogeochemistry and Ecosystem Research program (IMBER), to deliver a uni-

formly quality-controlled surface ocean $CO_2$ database. We cordially thank SOLAS (in particular Emilie Brevière) for kindly supporting the SOCOM kick-off meeting in Beijing (June 2013), and NIES (in particular Shin-ichiro Nakaoka and Yukihiro Nojiri) for kindly organizing and supporting the SOCOM progress meeting in Tsukuba (February 2015). We thank Amanda Fay for her advice in using the biome map, and Martin Heimann for helpful comments on the manuscript. The comments by our editor Victor Brovkin and two anonymous referees greatly helped us to make the manuscript more focused and accessible. We are grateful to Peter Brown for designing the SOCOM logo. N.M., N.G., and P.L. thank the EU FP7 project CARBOCHANGE (264879) for their support. N.G. and P.L. also acknowledge funding from the EU FP7 project GEOCARBON (283080). J.D.S. gratefully acknowledges support by the European Space Agency project contract No. 4000112091/14/I-LG, and thanks Peter Land for his help in data preparation. A.R.J. and K.B.R. have been kindly supported by NASA grant NNX14AL85G. The contribution of K.B. Rodgers came through awards NA17RJ2612 and NA08OAR4320752, which includes support through the NOAA Office of Climate Observations (OCO). P.P. thanks the EU FP7 project CARBONES and Abdou Kane for the construction of the neural network to derive the *CARBONES-NN* product. A.O. appreciates support from the Norwegian Research Council (SNACS: 229752).

## References

Bakker, D. C. E., Pfeil, B., Smith, K., Hankin, S., Olsen, A., Alin, S. R., Cosca, C., Harasawa, S., Kozyr, A., Nojiri, Y., O'Brien, K. M., Schuster, U., Telszewski, M., Tilbrook, B., Wada, C., Akl, J., Barbero, L., Bates, N. R., Boutin, J., Bozec, Y., Cai, W.-J., Castle, R. D., Chavez, F. P., Chen, L., Chierici, M., Currie, K., de Baar, H. J. W., Evans, W., Feely, R. A., Fransson, A., Gao, Z., Hales, B., Hardman-Mountford, N. J., Hoppema, M., Huang, W.-J., Hunt, C. W., Huss, B., Ichikawa, T., Johannessen, T., Jones, E. M., Jones, S. D., Jutterström, S., Kitidis, V., Körtzinger, A., Landschützer, P., Lauvset, S. K., Lefèvre, N., Manke, A. B., Mathis, J. T., Merlivat, L., Metzl, N., Murata, A., Newberger, T., Omar, A. M., Ono, T., Park, G.-H., Paterson, K., Pierrot, D., Ríos, A. F., Sabine, C. L., Saito, S., Salisbury, J., Sarma, V. V. S. S., Schlitzer, R., Sieger, R., Skjelvan, I., Steinhoff, T., Sullivan, K. F., Sun, H., Sutton, A. J., Suzuki, T., Sweeney, C., Takahashi, T., Tjiputra, J., Tsurushima, N., van Heuven, S. M. A. C., Vandemark, D., Vlahos, P., Wallace, D. W. R., Wanninkhof, R., and Watson, A. J.: An update to the Surface Ocean $CO_2$ Atlas (SOCAT version 2), Earth System Science Data, 6, 69–90, 2014.

Bakker, D. C. E., Pfeil, B., Smith, K., Harasawa, S., Landa, C., Nakaoka, S., Nojiri, Y., Metzl, N., O'Brien, K. M., Olsen, A., Schuster, U., Tilbrook, B., Wanninkhof, R., Alin, S. R., Barbero, L., Bates, N. R., Bianchi, A. A., Bonou, F., Boutin, J., Bozec, Y., Burger, E., Cai, W.-J., Castle, R. D., Chen, L., Chierici, M., Cosca, C., Currie, K., Evans, W., Featherstone, C., Feely, R. A., Fransson, A., Greenwood, N., Gregor, L., Hankin, S., Hardman-Mountford, N. J., Harlay, J., Hauck, J., Hoppema, M., Humphreys, M., Hunt, C. W., Ibánhez, J. S. P., Johannessen, T., Jones, S. D., Keeling, R., Kitidis, V., Körtzinger, A., Kozyr, A., Krasakopolou, E., Kuwata, A., Landschützer, P., Lauvset, S. K., Lefèvre, N., LoMonaco, C., Manke, A. B., Mathis, J. T., Merlivat, L., Monteiro, P., Munro, D., Murata, A., Newberger, T., Omar, A. M., Ono, T., Paterson, K., Pierrot, D., Robbins, L. L., Sabine, C. L., Saito, S., Salisbury, J., Schneider, B., Schlitzer, R., Sieger, R., Skjelvan, I., Steinhoff, T., Sullivan, K. F., Sutherland, S. C., Sutton, A. J., Sweeney, C., Tadokoro, K., Takahashi, T., Telszewski, M., Van Heuven, S. M. A. C., Vandemark, D., Wada, C., Ward, B., and Watson, A. J.: A 58-year record of high quality data in version 3 of the Surface Ocean $CO_2$ Atlas (SOCAT), Earth System Science Data, in preparation.

Claustre, H., Bishop, J., Boss, E., Bernard, S., Berthon, J.-F., Coatanoan, C., Johnson, K., Lotiker, A., Ulloa, O., Perry, M. J., D'Ortenzio, F., D'andon, O. H. F., and Uitz, J.: Bio-optical Profiling Floats as New Observational Tools for Biogeochemical and Ecosystem Studies, in Proceedings of OceanObs'09: Sustained Ocean Observations and Information for Society (Vol. 2), Venice, Italy, 21-25 September 2009, Hall, J., Harrison, D.E. and Stammer, D. (Eds.), ESA Publication WPP-306, 2010.

Cressman, G. P.: An operational objective analysis system, Mon. Weather Rev., 87, 367–374, 1959.

Delworth, T. L., Broccoli, A. J., Rosati, A., Stouffer, R. J., Balaji, V., Beesley, J. A., Cooke, W. F., Dixon, K. W., Dunne, J., Dunne, K. A., Durachta, J. W., Findell, K. L., Ginoux, P., Gnanadesikan, A., Gordon, C. T., Griffies, S. M., Gudgel, R., Harrison, M. J., Held, I. M., Hemler, R. S., Horowitz, L. W., Klein, S. A., Knutson, T. R., Kushner, P. J., Langenhorst, A. R., Lee, H.-C., Lin, S.-J., Lu, J., Malyshev, S. L., Milly, P. C. D., Ramaswamy, V., Russell, J., Schwarzkopf, M. D., Shevliakova, E., Sirutis, J. J., Spelman, M. J., Stern, W. F., Winton, M., Wittenberg, A. T., Wyman, B., Zeng, F., and Zhang, R.: GFDL's CM2 Global coupled climate models. Part I: Formulation and simulation characteristics, J. Clim., 19, 643–674, 2006.

Fay, A. R. and McKinley, G. A.: Global open-ocean biomes: mean and temporal variability, Earth System Science Data, 6, 273–284, 2014.

Feely, R. A., Wanninkhof, R., Takahashi, T., and Tans, P.: Influence of El Niño on the equatorial Pacific contribution to atmospheric $CO_2$ accumulation, Nature, 398, 597–601, 1999.

Galbraith, E., Kwon, E. Y., Gnanadesikan, A., Rodgers, K. B., Griffies, S. M., Bianchi, D., Sarmiento, J. L., Dunne, J. P., Simeon, J., Slater, R. D., Wittenberg, A. T., and Held, I. M.: Climate variability and radiocarbon in the CM2Mc Earth system model, J. Clim., 21, 4749–4765, 2011.

Gloor, M., Gruber, N., Sarmiento, J., Sabine, C. L., Feely, R. A., and Rödenbeck, C.: A first estimate of present and preindustrial air-sea $CO_2$ flux patterns based on ocean interior carbon measurements and models, Geophysical Research Letters, 30, 1010, 2003.

Gnanadesikan, A., Dixon, K., Griffies, S., Balaji, V., Barreiro, M., Beesley, J. A., Cooke, W. F., Delworth, T. L., Gerdes, R., Harrison, M. J., Held, I. M., Hurlin, W. J., Lee, H.-C., Liang, Z., Nong, G., Pacanowski, R. C., Rosati, A., Russell, J., Samuels, B. L., Song, Q., Spelman, M. J., Stouffer, R. J., Sweeney, C. O., Vecchi, G., Winton, M., Wittenberg, A. T., Zeng, F., Zhang, R., and Dunne, J. P.: GFDL's CM2 global coupled climate models. Part II: The baseline ocean simulation, J. Clim., 19, 675–697, 2006.

Goddijn-Murphy, L. M., Woolf, D. K., Land, P. E., Shutler, J. D., and Donlon, C.: The OceanFlux Greenhouse Gases methodology for deriving a sea surface climatology of $CO_2$ fugacity in support of air–sea gas flux studies, Ocean Science, 11, 519–541, 2015.

Griffies, S., Harrison, M., Pacanowski, R., and Rosati, A.: A technical guide to MOM4, Tech. Rep., NOAA GFDL, Princeton, NJ, 2004.

Gruber, N., Gloor, M., Fletcher, S. E. M., Doney, S. C., Dutkiewicz, S., Follows, M. J., Gerber, M., Jacobson, A. R., Joos, F., Lindsay, K., Menemenlis, D., Mouchet, A., Müller, S. A., Sarmiento, J. L., and Takahashi, T.: Oceanic sources, sinks, and transport of atmospheric $CO_2$, Global Biogeochem. Cycles, 23, GB1005, 2009.

Iida, Y., Kojima, A., Takatani, Y., Nakano, T., Midorikawa, T., and Ishii, M.: Trends in $pCO_2$ and sea-air $CO_2$ flux over the global open oceans for the last two decades., Journal of Oceanography, DOI 10.1007/s10872-015-0306-4, 2015.

Jacobson, A. R., Mikaloff Fletcher, S. E., Gruber, N., Sarmiento, J. L., and Gloor, M.: A joint atmosphere-ocean inversion for surface fluxes of carbon dioxide: 1. Methods and global-scale fluxes, Global Biogeochemical Cycles, 21, GB1019, 2007.

Jacobson et al.: Trends in surface ocean $pCO_2$, Global Biogeochemical Cycles, in preparation.

Jones, S. D., Le Quéré, C., and Rödenbeck, C.: Autocorrelation characteristics of surface ocean $pCO_2$ and air-sea $CO_2$ fluxes, Global Biogeochem. Cycles, 26, GB2042, 2012.

Jones, S. D., Quéré, C. L., Rödenbeck, C., Manning, A. C., and Olsen, A.: A statistical gap-filling method to interpolate global monthly surface ocean carbon dioxide data, J. Adv. Model. Earth Syst., 07, doi:10.1002/2014MS000 416, 2015.

Kalnay, E., Kanamitsu, M., Kistler, R., Collins, W., Deaven, D., Gandin, L., Iredell, M., Saha, S., White, G., Woollen, J., Zhu, Y., Chelliah, M., Ebisuzaki, W., Higgins, W., Janowiak, J., Mo, K. C., Ropelewski, C., Wang, J., Leetmaa, A., Reynolds, R., Jenne, R., and Joseph, D.: The NCEP/NCAR 40-year reanalysis project, Bull. Am. Met. Soc., 77, 437–471, 1996.

Khatiwala, S., Tanhua, T., Mikaloff Fletcher, S., Gerber, M., Doney, S. C., Graven, H. D., Gruber, N., McKinley, G. A., Murata, A., Ríos, A. F., and Sabine, C. L.: Global ocean storage of anthropogenic carbon, Biogeosciences, 10, 2169–2191, 2013.

Kurihara, Y., Sakurai, T., and Kuragano, T.: Global daily sea surface temperature analysis using data from satellite microwave radiometer, satellite infrared radiometer and in-situ observations., Sokko-jiho 73 S1-S18 (in Japanese), 2006.

Landschützer, P., Gruber, N., Bakker, D. C. E., Schuster, U., Nakaoka, S., Payne, M. R., Sasse, T., and Zeng, J.: A neural network-based estimate of the seasonal to inter-annual variability of the Atlantic Ocean carbon sink, Biogeosciences, 10, 7793–7815, 2013.

Landschützer, P., Gruber, N., Bakker, D. C. E., and Schuster, U.: Recent variability of the global ocean carbon sink, Global Biogeochemical Cycles, 28, 927–949, 2014.

Landschützer, P., Gruber, N., Haumann, F., Rödenbeck, C., Bakker, D., van Heuven, S., Hoppema, M., Metzl, N., Sweeney, C., Takahashi, T., Tilbrook, B., and Wanninkhof, R.: The reinvigoration of the Southern Ocean carbon sink, Science, 349, 1221–1224, 2015.

Large, W. and Yeager, S.: The global climatology of an interannually varying air-sea flux data set, Clim. Dyn., 33, 341–364, 2009.

Le Quéré, C., Moriarty, R., Andrew, R. M., Peters, G. P., Ciais, P., Friedlingstein, P., Jones, S. D., Sitch, S., Tans, P., Arneth, A., Boden, T. A., Bopp, L., Bozec, Y., Canadell, J. G., Chini, L. P., Chevallier, F., Cosca, C. E., Harris, I., Hoppema, M., Houghton, R. A., House, J. I., Jain, A. K., Johannessen, T., Kato, E., Keeling, R. F., Kitidis, V., Klein Goldewijk, K., Koven, C., Landa, C. S., Landschützer, P., Lenton, A., Lima, I. D., Marland, G., Mathis, J. T., Metzl, N., Nojiri, Y., Olsen, A., Ono, T., Peng, S., Peters, W., Pfeil, B., Poulter, B., Raupach, M. R., Regnier, P., Rödenbeck, C., Saito, S., Salisbury, J. E., Schuster, U., Schwinger, J., Séférian, R., Segschneider, J., Steinhoff, T., Stocker, B. D., Sutton, A. J., Takahashi, T., Tilbrook, B., van der Werf, G. R., Viovy, N., Wang, Y.-P., Wanninkhof, R., Wiltshire, A., and Zeng, N.: Global carbon budget 2014, Earth System Science Data, 7, 47–85, 2015.

Levitus, S.: Climatological atlas of the world ocean, United States Government Printing, Rockville, Md, 1982.

Majkut, J. D., Sarmiento, J. L., and Rodgers, K. B.: A growing oceanic carbon uptake: Results from an inversion study of surface $pCO_2$ data, Global Biogeochem. Cycles, 28, 335–351, 2014.

Manning, A. C. and Keeling, R. F.: Global oceanic and land biotic carbon sinks from the Scripps atmospheric oxygen flask sampling network, Tellus Series B-Chemical and Physical Meteorology, 58, 95–116, 2006.

Masarie, K. A. and Tans, P. P.: Extension and integration of atmospheric carbon dioxide data into a globally consistent measurement record, J. Geophys. Res., 100, 11 593–11 610, 1995.

Matsumoto, K., Sarmiento, J. L., Key, R. M., Aumont, O., Bullister, J. L., Caldeira, K., Campin, J.-M., Doney, S. C., Drange, H., Dutay, J.-C., Follows, M., Gao, Y., Gnanadesikan, A., Gruber, N., Ishida, A., Joos, F., Lindsay, K., Maier-Reimer, E., Marshall, J. C., Matear, R. J., Monfray, P., Mouchet, A., Najjar, R., Plattner, G.-K., Schlitzer, R., Slater, R., Swathi, P. S., Totterdell, I. J., Weirig, M.-F., Yamanaka, Y., Yool, A., and Orr, J. C.: Evaluation of ocean carbon cycle models with data-based metrics, Geophys. Res. Lett., 31, L07 303, 2004.

McKinley, G. A., Follows, M. J., and Marshall, J.: Mechanism of air-sea $CO_2$ flux variability in the equatorial Pacific and North Atlantic, Global Biogeochem. Cycles, 18, GB2011, doi:10.1029/2003GB002 179, 2004.

Naegler, T.: Reconciliation of excess $^{14}C$-constrained global $CO_2$ piston velocity estimates, Tellus, 61B, 372–384, 2009.

Nakaoka, S., Telszewski, M., Nojiri, Y., Yasunaka, S., Miyazaki, C., Mukai, H., and Usui, N.: Estimating temporal and spatial variation of ocean surface $pCO_2$ in the North Pacific using a self-organizing map neural network technique, Biogeosciences, 10, 6093–6106, 2013.

Orr, J. C., Najjar, R., Sabine, C. L., and Joos, F.: Abiotic-HOWTO, LSCE/CEA Saclay, Gif-sur-Yvette, France, 25 pp., 1999.

Park, G.-H., Wanninkhof, R., Doney, S. C., Takahashi, T., Lee, K., Feely, R. A., Sabine, C. L., Triñanes, J., and Lima, I. D.: Variability of global net sea-air $CO_2$ fluxes over the last three decades using empirical relationships, Tellus B, 62, 352–368, 2010a.

Park, G.-H., Wanninkhof, R., and Trinanes, J.: Procedures to Create Near Real-Time Seasonal Air-Sea $CO_2$ Flux Maps, Atlantic Oceanographic and Meteorological Laboratory, NOAA Technical Memorandum-98, OAR AOML, Miami, 2010b.

Peylin, P., Law, R. M., Gurney, K. R., Chevallier, F., Jacobson, A. R., Maki, T., Niwa, Y., Patra, P. K., Peters, W., Rayner, P. J., Rödenbeck, C., van der Laan-Luijkx, I. T., and Zhang, X.: Global atmospheric carbon budget: results from an ensemble of atmospheric $CO_2$ inversions, Biogeosciences, 10, 6699–6720, 2013.

Rödenbeck, C.: Estimating $CO_2$ sources and sinks from atmospheric mixing ratio measurements using a global inversion of atmospheric transport, Tech. Rep. 6, Max Planck Institute for Biogeochemistry, Jena, Germany, 2005.

Rödenbeck, C., Keeling, R. F., Bakker, D. C. E., Metzl, N., Olsen, A., Sabine, C., and Heimann, M.: Global surface-ocean $pCO_2$ and sea–air $CO_2$ flux variability from an observation-driven ocean mixed-layer scheme, Ocean Science, 9, 193–216, 2013.

Rödenbeck, C., Bakker, D. C. E., Metzl, N., Olsen, A., Sabine, C., Cassar, N., Reum, F., Keeling, R. F., and Heimann, M.: Interannual sea–air $CO_2$ flux variability from an observation-driven ocean mixed-layer scheme, Biogeosciences, 11, 4599–4613, 2014.

Rodgers, K., Aumont, O., Mikaloff Fletcher, S., Plancherel, Y., Bopp, L., de Boyer Montégut, C., Iudicone, D., Keeling, R., Madec, G., and Wanninkhof, R.: Strong sensitivity of Southern Ocean carbon uptake and nutrient cycling to wind stirring, Biogeosciences, 11, 4077–4098, 2014.

Sabine, C. L., Feely, R. A., Gruber, N., Key, R. M., Lee, K., Bullister, J. L., Wanninkhof, R., Wong, C. S., Wallace, D. W. R., Tilbrook, B., Millero, F. J., Peng, T.-H., Kozyr, A., Ono, T., and Rios, A.: The Oceanic Sink for Anthropogenic $CO_2$, Science, 305, 367–371, 2004.

Sabine, C. L., Hankin, S., Koyuk, H., Bakker, D. C. E., Pfeil, B., Olsen, A., Metzl, N., Kozyr, A., Fassbender, A., Manke, A., Malczyk, J., Akl, J., Alin, S. R., Bellerby, R. G. J., Borges, A., Boutin, J., Brown, P. J., Cai, W.-J., Chavez, F. P., Chen, A., Cosca, C., Feely, R. A., González-Dávila, M., Goyet, C., Hardman-Mountford, N., Heinze, C., Hoppema, M., Hunt, C. W., Hydes, D., Ishii, M., Johannessen, T., Key, R. M., Körtzinger, A., Landschützer, P., Lauvset, S. K., Lefèvre, N., Lenton, A., Lourantou, A., Merlivat, L., Midorikawa, T., Mintrop, L., Miyazaki, C., Murata, A., Nakadate, A., Nakano, Y., Nakaoka, S., Nojiri, Y., Omar, A. M., Padin, X. A., Park, G.-H., Paterson, K., Perez, F. F., Pierrot, D., Poisson, A., Ríos, A. F., Salisbury, J., Santana-Casiano, J. M., Sarma, V. V. S. S., Schlitzer, R., Schneider, B., Schuster, U., Sieger, R., Skjelvan, I., Steinhoff, T., Suzuki, T., Takahashi, T., Tedesco, K., Telszewski, M., Thomas, H., Tilbrook, B., Vandemark, D., Veness, T., Watson, A. J., Weiss, R., Wong, C. S., and Yoshikawa-Inoue, H.: Surface Ocean $CO_2$ Atlas (SOCAT) gridded data products, Earth System Science Data, 5, 145–153, 2013.

Sasse, T. P., McNeil, B. I., and Abramowitz, G.: A new constraint on global air-sea $CO_2$ fluxes using bottle carbon data, Geophys. Res. Lett., 40, 1594–1599, 2013.

Schuster, U., Watson, A. J., Bates, N. R., Corbière, A., González-Dávila, M., Metzl, N., Pierrot, D., and Santana-Casiano, J. M.: Trends in North Atlantic sea-surface $fCO_2$ from 1990 to 2006, Deep Sea Res. II, 56, 620–629, 2009.

Schuster, U., McKinley, G. A., Bates, N., Chevallier, F., Doney, S. C., Fay, A. R., González-Dávila, M., Gruber, N., Jones, S., Krijnen, J., Landschützer, P., Lefèvre, N., Manizza, M., Mathis, J., Metzl, N., Olsen, A., Rios, A. F., Rödenbeck, C., Santana-Casiano, J. M., Takahashi, T., Wanninkhof, R., and Watson, A. J.: Atlantic and Arctic sea-air $CO_2$ fluxes, 1990-2009, Biogeosciences, 10, 607–627, 2013.

Séférian, R., Ribes, A., and Bopp, L.: Detecting the anthropogenic influences on recent changes in ocean carbon uptake, Geophysical Research Letters, 41, 5968–5977, doi: 10.1002/2014GL061 223, 2014.

Shutler, J. D., Land, P. E., Piolle, J.-F., Woolf, D. K., Goddijn-Murphy, L., Paul, F., Girard-Ardhuin, F., Chapron, B., and Donlon, C.: FluxEngine: A flexible processing system for calculating atmosphere-ocean carbon dioxide gas fluxes and climatologies, Journal of Atmospheric and Oceanic Technology, in revision.

Stocker, T., Qin, D., Plattner, G.-K., Tignor, M., Allen, S., Boschung, J., Nauels, A., Xia, Y., Bex, V., and Midgley, P., eds.: Climate Change 2013: The Physical Science Basis. Contribution of Working Group I to the Fifth Assessment Report of the Intergovernmental Panel on Climate Change, Cambridge University Press, Cambridge, United Kingdom and New York, NY, USA, 2013.

Takahashi, T., Sutherland, S., and Kozyr, A.: Global ocean surface water partial pressure of $CO_2$ database: Measurements performed during 1968-2006 (Version 1.0). ORNL/CDIAC-152, NDP-088, Carbon Dioxide Information Analysis Center, Oak Ridge National Laboratory, U.S. Department of Energy, Oak Ridge, Tennessee, 20 pp., 2007.

Takahashi, T., Sutherland, S. C., Wanninkhof, R., Sweeney, C., Feely, R. A., Chipman, D. W., Hales, B., Friederich, G., Chavez, F., Sabine, C., Watson, A., Bakker, D. C. E., Schuster, U., Metzl, N., Yoshikawa-Inoue, H., Ishii, M., Midorikawa, T., Nojiri, Y., Kortzinger, A., Steinhoff, T., Hoppema, M., Olafsson, J., Arnarson, T. S., Tillbrook, B., Johannessen, T., Olsen, A., Bellerby, R., Wong, C. S., Delille, B., Bates, N. R., and de Baar, H. J. W.: Climatological mean and decadal change in surface ocean $pCO_2$ and net sea-air $CO_2$ flux over the global oceans, Deep-Sea Res. II, 56, 554–577, 2009.

Takahashi, T., Sutherland, S., and Kozyr, A.: GLobal ocean surface water partial pressure of $CO_2$ database, Measurements performed during 1957-2011 (version 2011), ORNL/CDIAC-160, NDP-088(V2011), Carbon Dioxide Information Analysis Center, Oak Ridget National Laboratory, U.S. Department of Energy, Oak Ridge, Tennessee, 2012.

Takahashi, T., Sutherland, S., and Kozyr, A.: Global ocean surface water partial pressure of $CO_2$ database: Measurements performed during 1957-2013 (Version 2013). ORNL/CDIAC-160, NDP-088(V2013), Carbon Dioxide Information Analysis Center, Oak Ridge National Laboratory, U.S. Department of Energy, Oak Ridge, Tennessee, 2014a.

Takahashi, T., Sutherland, S. C., Chipman, D. W., Goddard, J. G., Newberger, T., and Sweeney, C.: Climatological Distributions of pH, $pCO_2$, Total $CO_2$, Alkalinity, and $CaCO_3$ Saturation in the Global Surface Ocean, ORNL/CDIAC-160, NDP-094. Carbon Dioxide Information Analysis Center, Oak Ridge National Laboratory, U.S. Department of Energy, Oak Ridge, Tennessee. doi: 10.3334/CDIAC/OTG.NDP094, 2014b.

Turi, G., Lachkar, Z., and Gruber, N.: Spatiotemporal variability and drivers of $pCO_2$ and air-sea $CO_2$ fluxes in the California Current System: an eddy-resolving modelling study, Biogeosciences, 11, 671–690, 2014.

Uppala, S. M., Kållberg, P. W., Simmons, A. J., Andrae, U., Bechtold, V. D. C., Fiorino, M., Gibson, J. K., Haseler, J., Hernandez, A., Kelly, G. A., Li, X., Onogi, K., Saarinen, S., Sokka, N., Allan, R. P., Andersson, E., Arpe, K., Balmaseda, M. A., Beljaars, A. C. M., Berg, L. V. D., Bidlot, J., Bormann, N., Caires, S., Chevallier, F., Dethof, A., Dragosavac, M., Fisher, M., Fuentes, M., Hagemann, S., Hólm, E., Hoskins, B. J., Isaksen, L., Janssen,

P. A. E. M., Jenne, R., Mcnally, A. P., Mahfouf, J.-F., Morcrette, J.-J., Rayner, N. A., Saunders, R. W., Simon, P., Sterl, A., Trenberth, K. E., Untch, A., Vasiljevic, D., Viterbo, P., , and Woollen, J.: The ERA-40 re-analysis, Q.J.R. Meteorolog. Soc., 131, 2961–3012, 2005.

U.S. Department Commerce: 2-minute gridded global relief data (ETOPO2v2), Natl. Oceanic and Atmos. Admin., Natl. Geophys. Data Cent. [Available at http://www.ngdc.noaa.gov/mgg/fliers/06mgg01.html.], 2006.

Usui, N., Ishizaki, S., Fujii, Y., Tsujino, H., Yasuda, T., and Kamachi, M.: Meteorological Research Institute multivariate ocean variational estimation (MOVE) system: Some early results., Adv. Space Res., 37, 806–822, 2006.

Valsala, K. V. and Maksyutov, S.: Simulation and assimilation of global ocean $p\mathrm{CO_2}$ and air-sea $\mathrm{CO_2}$ fluxes using ship observations of surface ocean $p\mathrm{CO_2}$ in a simplified Biogeochemical offline model, Tellus, 62B, 821–840, 2010.

Valsala, K. V., Maksyutov, S., and Ikeda, M.: Design and validation of an offline oceanic tracer transport model for a carbon cycle study, J. Clim., 21, 2752–2769, 2008.

Wanninkhof, R.: Relationship between wind speed and gas exchange over the ocean, Journal of Geophysical Research-Oceans, 97, 7373–7382, 1992.

Wanninkhof, R., Park, G. H., Takahashi, T., Sweeney, C., Feely, R., Nojiri, Y., Gruber, N., Doney, S. C., McKinley, G. A., Lenton, A., Le Quéré, C., Heinze, C., Schwinger, J., Graven, H., and Khatiwala, S.: Global ocean carbon uptake: magnitude, variability and trends, Biogeosciences, 10, 1983–2000, 2013.

Wunsch, C., Heimbach, P., Ponte, R., Fukumori, I., and the ECCO-GODAE Consortium Members: The Global General Circulation of the Ocean Estimated by the ECCO-Consortium, Oceanography, 22, 88 103, 2009.

Yu, L. and Weller, R. A.: Objectively Analyzed air-sea heat Fluxes (OAFlux) for the global oceans, Bull. Am. Met. Soc., 88, 527–539, 2007.

Zeng, J., Nojiri, Y., Landschützer, P., Telszewski, M., and Nakaoka, S.: A global surface ocean $f\mathrm{CO_2}$ climatology based on a feed-forward neural network, Journal of Atmospheric and Ocean Technology, 31, 1838–1849, 2014.

Zeng, J., Nakajima, H., Nojiri, Y., and Nakaoka, S.: Reconstructing the Carbon Dioxide Absorption Patterns of World Oceans Using a Feed-Forward Neural Network: Software Implementation and Employment Techniques, 2015a.

Zeng, J., Nojiri, Y., Nakaoka, S., Nakajima, H., and Shirai, T.: Surface ocean $\mathrm{CO_2}$ in 1990-2011 modelled using a feed-forward neural network, Geoscience Data Journal, 2, 47–51, 2015b.

**Table 1.** General information on the mapping methods.

| | Version used | Contact | Reference | Method type |
|---|---|---|---|---|
| *UEA-SI* | v1.0 | Steve Jones | Jones et al. (2015) | Stat. Interpol. |
| *OceanFlux-SI* | v0.95 | Jamie Shutler | Shutler et al. (in revision) | Stat. Interpol. |
| *Jena-MLS* | oc_v1.3 | Christian Rödenbeck | update of Rödenbeck et al. (2014) | Stat. Interpol. |
| *CU-SCSE* | v1.0 | Andy Jacobson | Jacobson et al. (in preparation) | Stat. Interpol. |
| *AOML-EMP* | v2 | Geun-Ha Park | Park et al. (2010a) | Regression |
| *UEx-MLR* | v2.0 | Ute Schuster | Schuster et al. (2013) | Regression |
| *JMA-MLR* | v2 | Yosuke Iida | Iida et al. (2015) | Regression |
| *UNSW-SOMLO* | v1 | Tristan Sasse | Sasse et al. (2013) | Regression |
| *ETH-SOMFFN* | ETH30yr01 | Peter Landschützer | Landschützer et al. (2014) | Regression |
| *CARBONES-NN* | 2014-02-18 | Philippe Peylin | http://www.carbones.eu/wcmqs/ | Regression |
| *NIES-SOM* | v1.2 | Shin-ichiro Nakaoka | update of Nakaoka et al. (2013) | Regression |
| *NIES-NN* | v1.0 | Jiye Zeng | Zeng et al. (2014) | Regression |
| *PU-MCMC* | v1.0 | Keith Rodgers | Majkut et al. (2014) | Model-based |
| *NIES-OTTM* | 2013-08-11 | Vinu Valsala | Valsala and Maksyutov (2010) | Model-based |

**Table 2.** Original domains and grid resolutions of the products

| | Original domain –spatially[a] | –temporally | Original grid resolution –spatially | –temporally |
|---|---|---|---|---|
| *UEA-SI* | Global (up to 70° N) | 1985–2011 | $2.5^\circ \times 2.5^\circ$ | monthly |
| *OceanFlux-SI* | Global | 1995–2009 | $1^\circ \times 1^\circ$ | monthly |
| *Jena-MLS* | Global | 1987–2013 | $\approx 4^\circ \times 5^\circ$ | daily |
| *CU-SCSE* | Global | 1970–2011 | $1^\circ \times 1^\circ$ | monthly |
| *AOML-EMP* | Global | 1985–2011 | $\approx 4^\circ \times 5^\circ$ | monthly |
| *UEx-MLR* | Global | 1990–2012 | $1^\circ \times 1^\circ$ | monthly |
| *JMA-MLR* | Global | 1990–2012 (Chl IAV since 1997) | $1^\circ \times 1^\circ$ | monthly |
| *UNSW-SOMLO* | Global (open-ocean) | 1998–2011 | $1^\circ \times 1^\circ$ | monthly |
| *ETH-SOMFFN* | Global (up to 79° N) | 1982-2011 | $1^\circ \times 1^\circ$ | monthly |
| *CARBONES-NN* | Global | 1990–2009 | $2^\circ \times 2^\circ$ | monthly |
| *NIES-SOM* | Global | 1998–2009 | $1^\circ \times 1^\circ$ | monthly |
| *NIES-NN* | Global | 1990–2012 | $1^\circ \times 1^\circ$ | monthly |
| *PU-MCMC* | Global | 1980–2009 | $4^\circ \times 5^\circ$ | monthly |
| *NIES-OTTM* | Global | 1980–2010 | $1^\circ \times 1^\circ$ | monthly |

[a] Even if designated "global", most methods exclude some coastal areas or the Arctic, or treat coastal areas as open ocean.

**Table 3.** Specifications of the mapping methods with respect to the constraints and assumptions used (see Appendix A for details and references).

| | $pCO_2$ data | Adjusted variable | Coherence scales of adjustments[e] –spatially | –temporally | Regression of $pCO_2$ against[l] | Prescribed relation |
|---|---|---|---|---|---|---|
| *UEA-SI* | SOCATv2 | $pCO_2$ | Correlated pixels | 1–4 harmonics | -/- | -/- |
| *OceanFlux-SI* | SOCATv2 | $pCO_2$ | Correlated pixels | Correlated time steps | -/- | -/- |
| *Jena-MLS* | SOCATv3[k] | Internal C fluxes[c] | Correlated pixels | Correlated days | -/- | -/- |
| *CU-SCSE* | SOCATv2 | Pattern magnitudes | 10 ocean basins | Correlated time steps[g] | Spatial basis functions (EOFs based on models) | Linear |
| *AOML-EMP* | Takah. clim. | Regr. coeff. | Independent pixels | 1-4 sub-annual periods | SST | Linear |
| *UEx-MLR* | SOCATv2[a] | Regr. coeff. | 20 ocean regions | Entire period | SST, MLD, Chl, $pCO_2^{atm}$ | Linear |
| *JMA-MLR* | SOCATv2[b] | Regr. coeff. | 44 regions | Entire period | SST, SSS, Chl | Linear |
| *UNSW-SOMLO* | SOCATv2 | Regr. coeff. | Biogeochem. fingerprints[f] | Entire period | SST, SSS, MLD, Chl $xCO_2$ | Lin. (Non-lin.)[f] |
| *ETH-SOMFFN* | SOCATv2 | Network weights | Biogeochem. provinces | Entire period | SST, SSS, MLD, Chl, $xCO_2$ | Non-linear |
| *CARBONES-NN* | LDEOv1.0 | Network weights | Global | Moving window | SST, SSS, MLD, Chl, lat[h], long[h] | Non-linear |
| *NIES-SOM* | SOCATv2 | Assignments | Global | Entire period | SST, SSS, MLD, Chl, lat, long, time | Non-linear |
| *NIES-NN* | SOCATv2[a,b] | Network weights | Global | Entire period | SST, SSS, Chl, lat, long, month | Non-linear |
| *PU-MCMC* | LDEO2010 | Regr. coeff. | Independent pixels | Entire period | Mean, trend, seas., and IAV from model simulation | Scaled model |
| *NIES-OTTM* | LDEOv1.0 | IC + BC of DIC[d] | Independent pixels | 2-months windows | Various drivers through the process model | Model |

[a] plus additional recent data
[b] except some coastal data
[c] Ocean-internal sources and sinks of carbon to the mixed layer
[d] Initial and boundary conditions of the DIC field
[e] Spatial and temporal domains of the adjustable degrees of freedom. Roughly speaking, $pCO_2$ structures *within* these domains originate from the structures in the driving variables, while structures *between* these domains are directly determined by the $pCO_2$ data. Thus, the coherence scales determine the balance between the ability of a method to bridge data gaps and its ability to directly follow the observed signals.
[f] The fingerprints are derived by non-linear clustering of the data themselves, thus the mapping as a whole is non-linear.
[g] The individual basis functions have widely different relaxation time scales (3 months – 5 years).
[h] Only for step 1 (seasonality), not for step 2 (IAV)
[k] Values with flags A–D, not E
[l] Note that the data sets used for the same quantity may differ between the individual methods.
Glossary: Regr. coeff.=Regression coefficients, lat=latitude, long=longitude
Variables: Chl=Chlorophyll-a, MLD=Mixed layer depth, SSS=Sea Surface Salinity, SST=Sea Surface Temperature, $xCO_2$=Atmospheric $CO_2$ mixing ratio

**Table 4.** Information content about various modes of variability as implemented by the individual mapping methods. Modes labelled as "EST." (= estimated) are considered to reflect data-based information, as they either are directly estimated by time-dependent adjustments, or are regressed against drivers through multiple adjustable degrees of freedom. The trend is considered estimated if the interannual degrees of freedom allow a data-based trend to establish or if $pCO_2$ is explicitly regressed against a rising term (time or atmospheric $CO_2$).

| Method | Mean | Seasonality | IAV | Trend | Day-to-day |
|---|---|---|---|---|---|
| *UEA-SI* | EST. | EST. | partly est. | EST. | -/- |
| *OceanFlux-SI* | EST. | EST. | parameterized | prescribed | -/- |
| *Jena-MLS* | EST. | EST. | EST. | EST. | parameterized |
| *CU-SCSE* | EST. | EST. | EST. | EST. | interpolated |
| *AOML-EMP* | EST. | EST. | EST. | modelled | -/- |
| *UEx-MLR* | EST. | EST. | EST. | EST. | -/- |
| *JMA-MLR* | EST. | EST. | EST. | prescribed | -/- |
| *UNSW-SOMLO* | EST. | EST. | EST. | EST. | -/- |
| *ETH-SOMFFN* | EST. | EST. | EST. | EST. | -/- |
| *CARBONES-NN* | EST. | EST. | EST. | EST. | -/- |
| *NIES-SOM* | EST. | EST. | EST. | EST. | -/- |
| *NIES-NN* | EST. | EST. | EST. | EST. | -/- |
| *PU-MCMC* | EST. | scaled model | scaled model | EST. | -/- |
| *NIES-OTTM* | EST. | EST. | EST. | -/- | -/- |

**Table 5.** Biomes of Fay and McKinley (2014) used for time series comparison (see Fig. 2).

| No. | Abbreviation | Name |
|---|---|---|
| 1 | NP ICE | (omitted) North Pacific Ice |
| 2 | NP SPSS | North Pacific Subpolar Seasonally Stratified |
| 3 | NP STSS | North Pacific Subtropical Seasonally Stratified |
| 4 | NP STPS | North Pacific Subtropical Permanently Stratified |
| 5 | PEQU-W | West Pacific Equatorial |
| 6 | PEQU-E | East Pacific Equatorial |
| 7 | SP STPS | South Pacific Subtropical Permanently Stratified |
| 8 | NA ICE | (omitted) North Atlantic Ice |
| 9 | NA SPSS | North Atlantic Subpolar Seasonally Stratified |
| 10 | NA STSS | North Atlantic Subtropical Seasonally Stratified |
| 11 | NA STPS | North Atlantic Subtropical Permanently Stratified |
| 12 | AEQU | Atlantic Equatorial |
| 13 | SA STPS | South Atlantic Subtropical Permanently Stratified |
| 14 | IND STPS | Indian Ocean Subtropical Permanently Stratified |
| 15 | SO STSS | Southern Ocean Subtropical Seasonally Stratified |
| 16 | SO SPSS | Southern Ocean Subpolar Seasonally Stratified |
| 17 | SO ICE | Southern Ocean Ice |

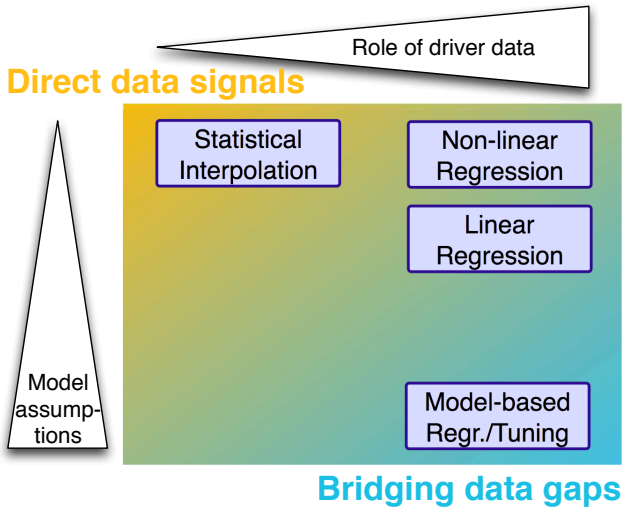


**Fig. 1.** Classes of $pCO_2$ mapping methods: *Statistical interpolation methods* essentially only use the $pCO_2$ data themselves, filling spatio-temporal gaps by assuming a statistical relation to neighbouring data points. In well-constrained areas/periods, they closely follow the signals contained in the data, while in areas/periods far from neighbouring data points, they remain essentially unconstrained. *Regression methods* establish a quantitative relation between $pCO_2$ and a set of external variables assumed to capture the major modes of spatio-temporal variability. Adjustable degrees of freedom are constant in time and within certain spatial regions, such that data gaps can be filled according to the spatio-temporal structure in the external variables; however, variability not contained in any of the chosen external data sets cannot be reproduced. Non-linear regression methods (feed-forward neural networks, self-organizing maps) essentially do not impose any structure to this relation between $pCO_2$ and the drivers. (Multi-)linear regression imposes a linear relationship, thereby restricting the type of responses but ensuring a unique and mathematically well-defined solution. Finally, knowledge of biogeochemical processes can be brought to bear by regression of $pCO_2$ against fields simulated by a *biogeochemical process model*, or by tuning initial conditions or parameters in such a model simulation to match the observations. However, this relies heavily on the structure of the process simulation to be correct.

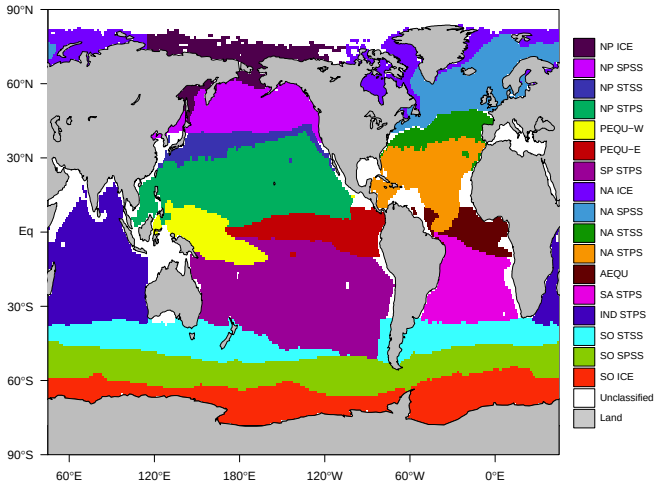


**Fig. 2.** Map of biomes (Fay and McKinley, 2014) used for time series comparison. (See Table 5 for biome names.)

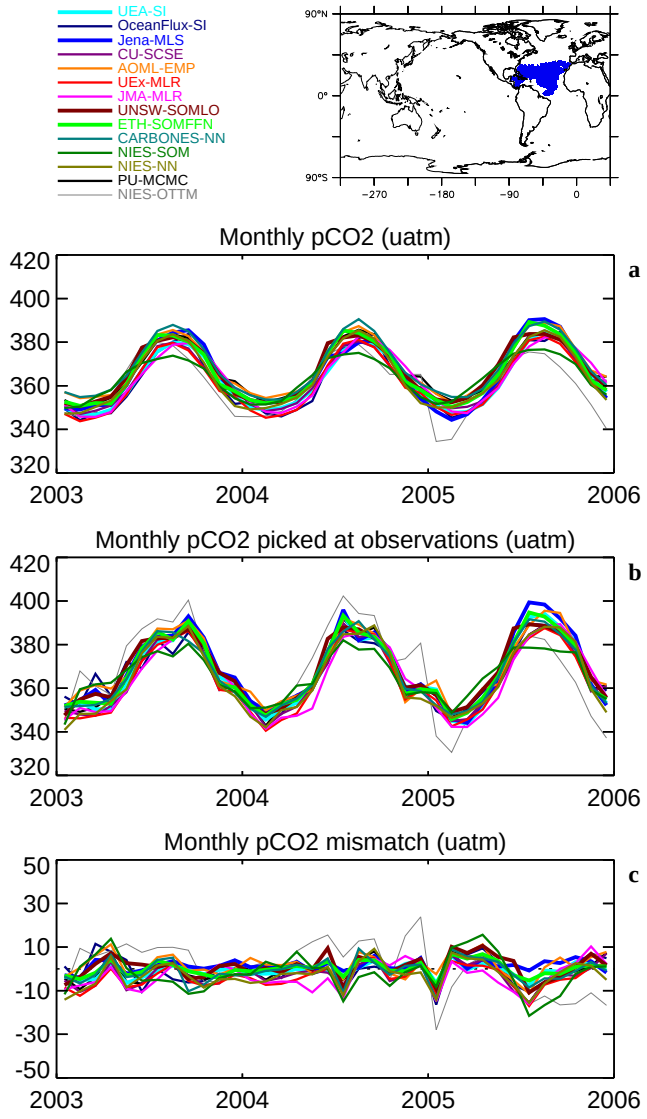


**Fig. 3.** $pCO_2$ time series from all 14 presented mapping methods averaged over the North Atlantic Subtropical Permanently Stratified biome of Fay and McKinley (2014, illustrated by the little map). Line styles indicate the relative monthly mismatch: $R^{\mathrm{month}} < 30\%$ (thick), 30–60% (medium), 60–75% (thin), above 75% (dashed).
**(a)** $pCO_2$ on monthly time steps for 3 selected years.
**(b)** As (a), but averages only calculated over pixels with data in the SOCATv2 monthly gridded data set.
**(c)** Mismatch: Biome-average difference between the submitted $pCO_2$ fields and the co-located SOCATv2 monthly gridded values.

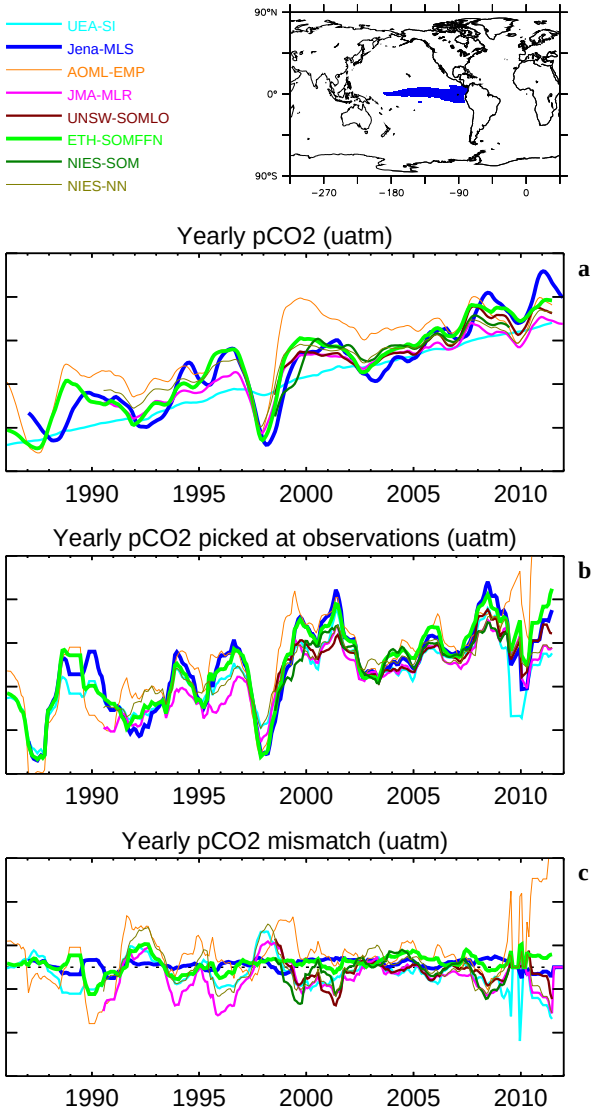


**Fig. 4.** $pCO_2$ time series from selected mapping methods (having a relative IAV mismatch $R^{\mathrm{iav}} < 75\%$) averaged over the East Pacific Equatorial biome of Fay and McKinley (2014, illustrated by the little map). Line styles indicate the relative IAV mismatch: $R^{\mathrm{iav}} < 30\%$ (thick), 30–60% (medium), 60–75% (thin).
**(a)** Interannual $pCO_2$ variations (12-months running mean).
**(b)** As (a), but averages only calculated over pixels with data in the SOCATv2 monthly gridded data set.
**(c)** Mismatch: Biome/yearly-average difference between the submitted $pCO_2$ fields and the co-located SOCATv2 monthly gridded values.

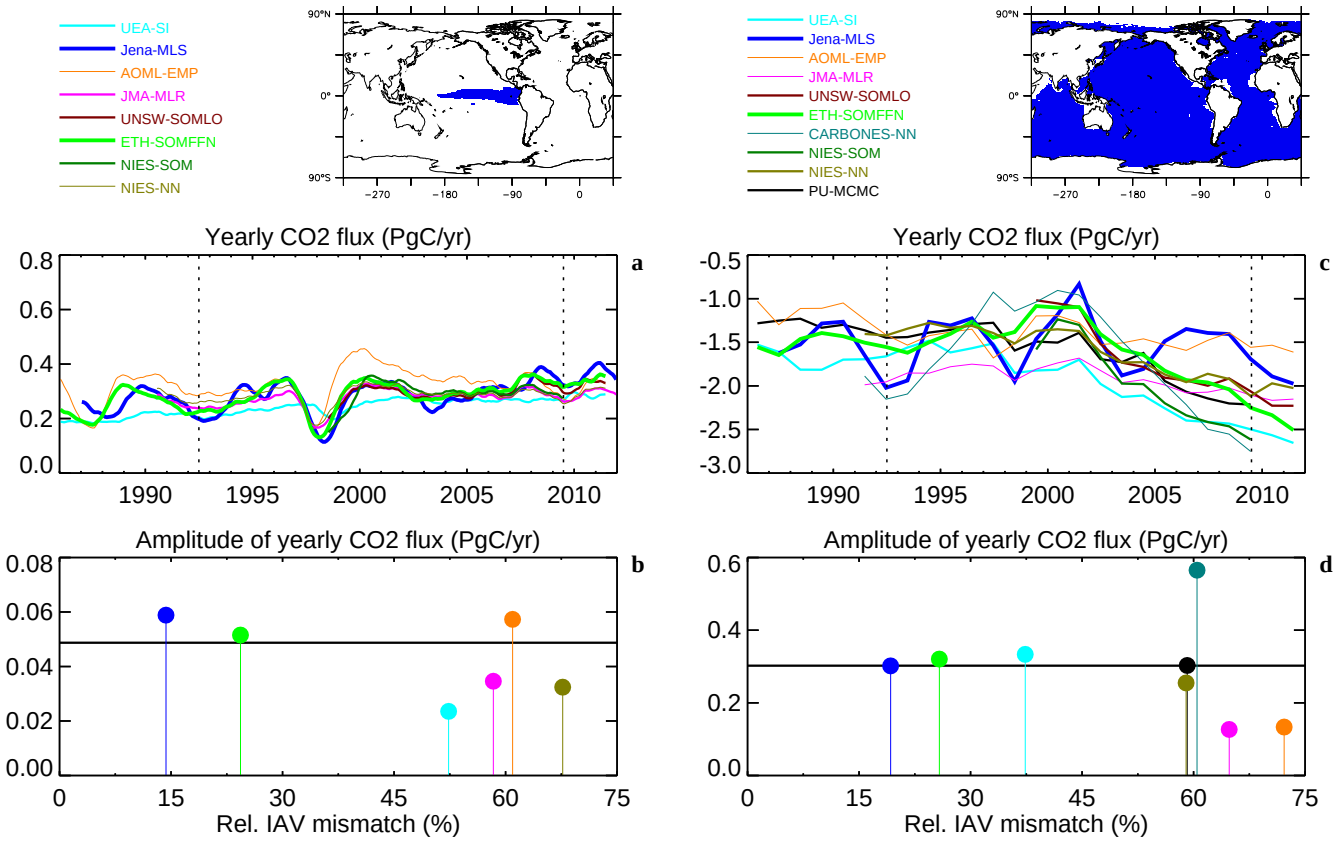


**Fig. 5.** Interannual sea–air $CO_2$ flux variations in the East Pacific Equatorial biome (left) and the global ocean (right) from selected mapping methods (having relative IAV mismatch $R^{\mathrm{iav}} < 75\%$ for $pCO_2$ averaged in the respective region). **(a,c)** Time series (yearly flux sum). Line styles indicate the relative IAV mismatch: $R^{\mathrm{iav}} < 30\%$ (thick), 30–60% (medium), 60–75% (thin). The vertical dotted lines delimit the analysis period for the amplitude computation. **(b,d)** Amplitudes $A_i^{\mathrm{iav}}$ of interannual $CO_2$ flux variations (see Sect. 4.2) plotted against the relative IAV mismatch amplitude $R_i^{\mathrm{iav}}$ for each submission (cases not fully covering the analysis period have been omitted to avoid inconsistencies). The weighted mean $\overline{A^{\mathrm{iav}}}$ (Eq. 3) is given as horizontal line.

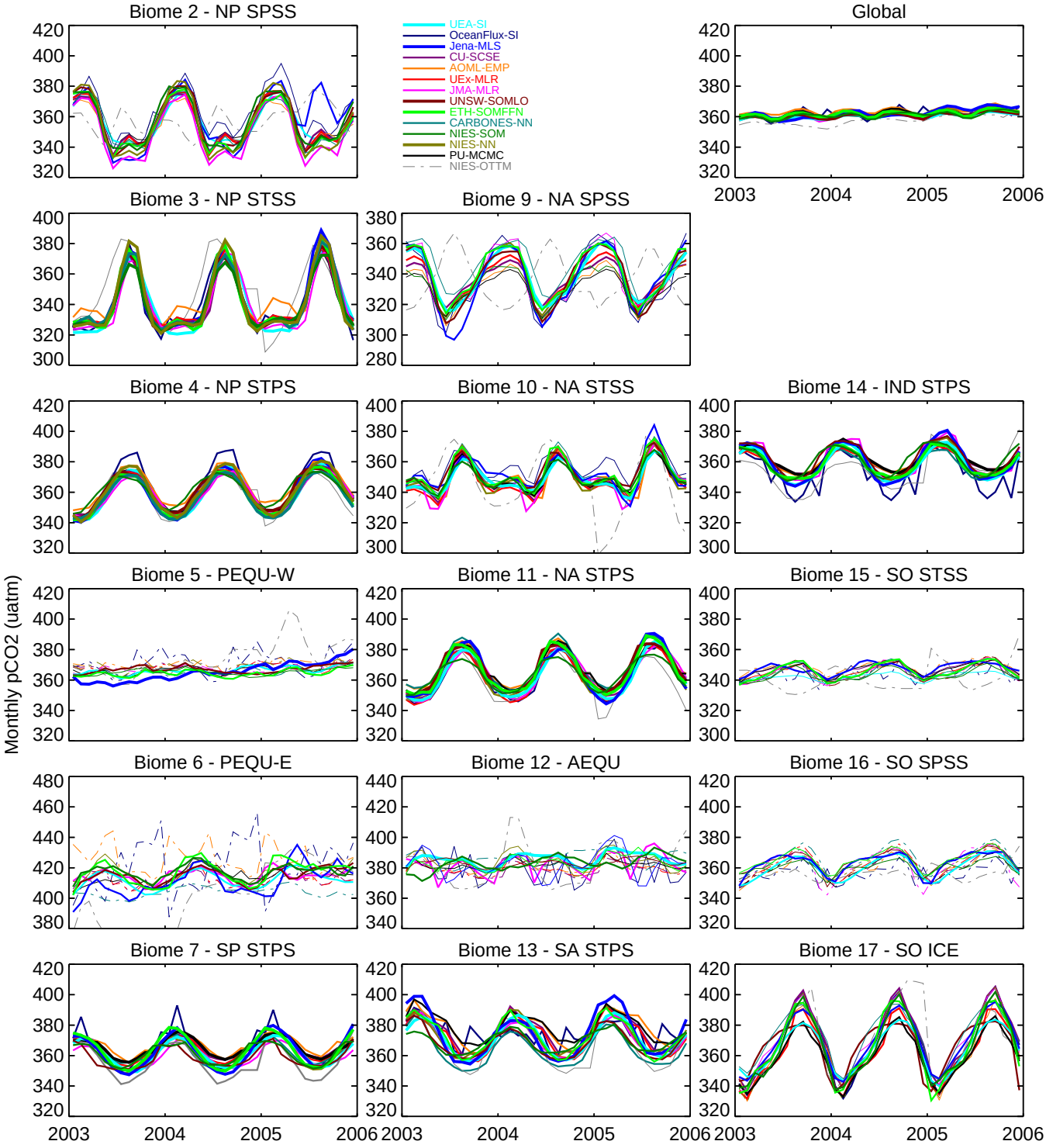


**Fig. A1.** Monthly $pCO_2$ variations over years 2003–2005 (arbitrarily selected) as estimated by all mapping methods, averaged over the biomes by Fay and McKinley (2014) (see Fig. 2, panels roughly in geographical arrangement). Vertical scales span the same range for all biomes ($100\,\mu\mathrm{atm}$), but some vertical shift has been chosen according to the mean spatial $pCO_2$ pattern. Line styles indicate the relative monthly mismatch: $R^{\mathrm{month}} < 30\%$ (thick), 30–60% (medium), 60–75% (thin), above 75% (dashed); the legend reflects "Global". In some biomes, lines of certain mapping methods with higher mismatches have been clipped (rather than enlarging the vertical scale), in order to maintain clarity. Biomes 1 (North Pacific Ice) and 8 (North Atlantic Ice) have been omitted due to extremely sparse data coverage.

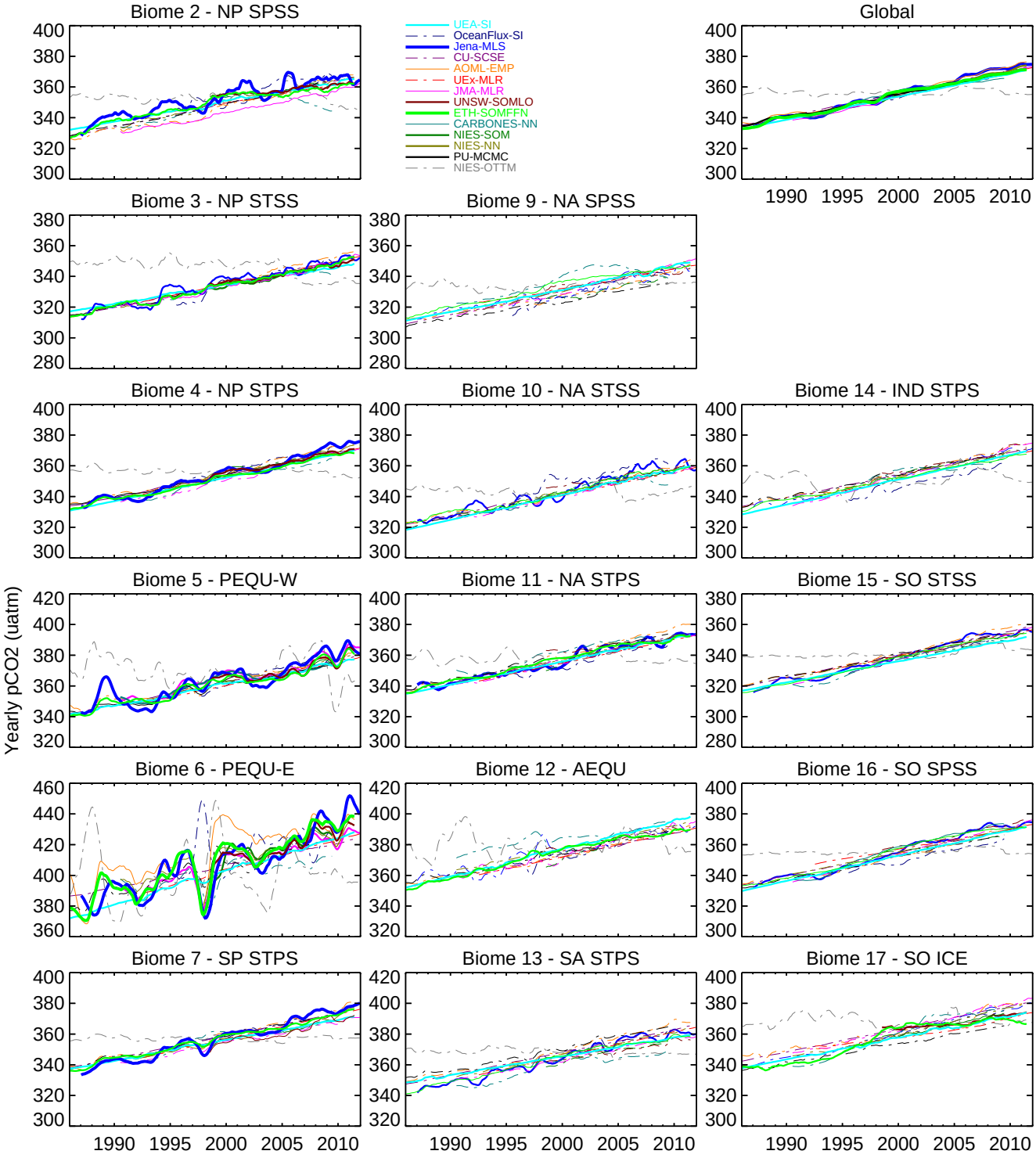


**Fig. A2.** Interannual $pCO_2$ variations as estimated by all mapping methods, averaged over the biomes by Fay and McKinley (2014) (see Fig. 2, panels roughly in geographical arrangement). Line styles indicate the relative IAV mismatch: $R^{\mathrm{iav}} < 30\%$ (thick), 30–60% (medium), 60–75% (thin), above 75% (dashed); the legend reflects "Global". Vertical scales span the same range for all biomes (100 µatm), but some vertical shift has been chosen according to the mean spatial $pCO_2$ pattern. In some biomes, lines of certain mapping methods with higher mismatches have been clipped (rather than enlarging the vertical scale), in order to maintain clarity. Biomes 1 (North Pacific Ice) and 8 (North Atlantic Ice) have been omitted due to extremely sparse data coverage.

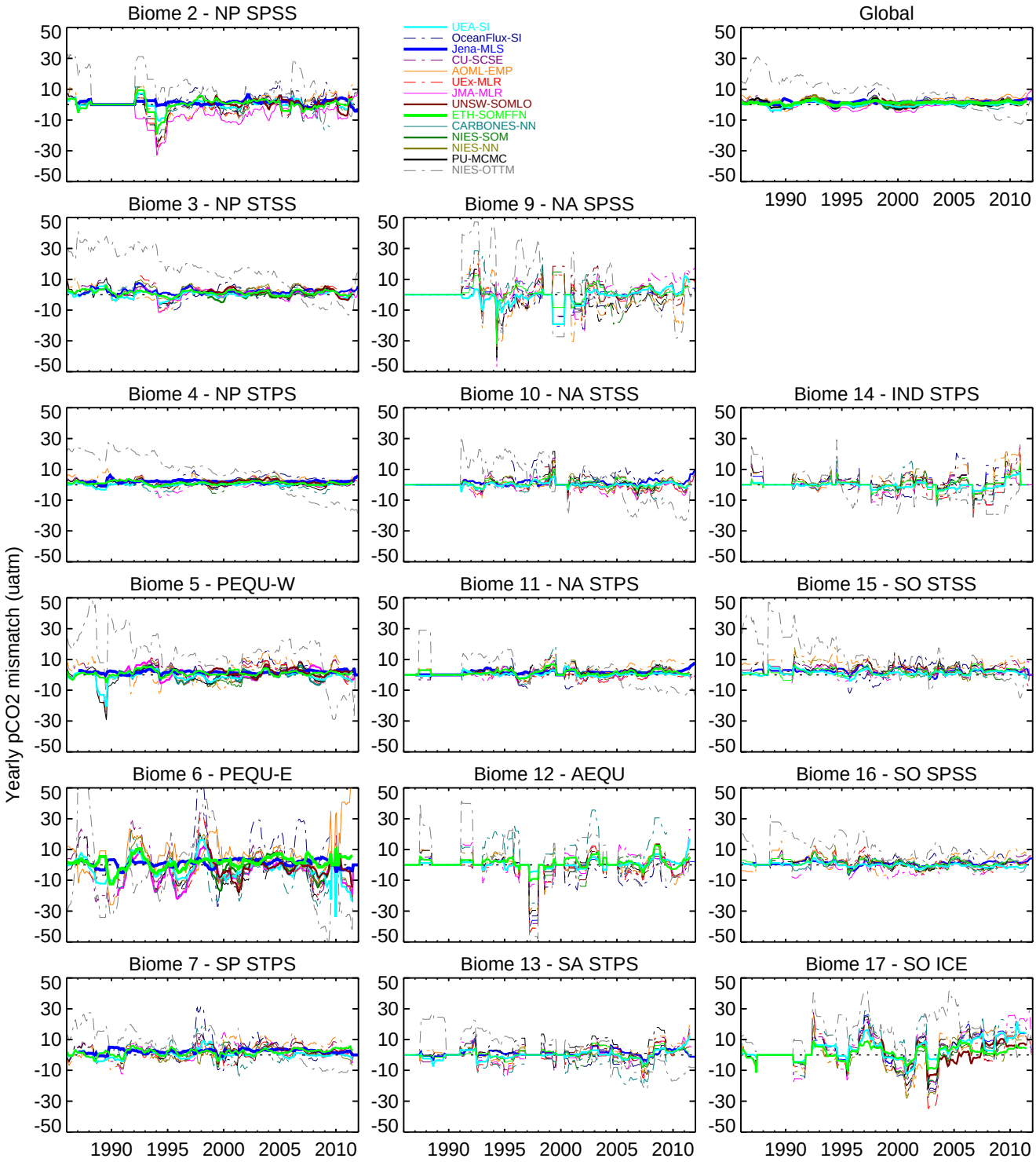


**Fig. A3.** Mismatch between the interannual $pCO_2$ variations as estimated by all mapping methods and the SOCATv2 monthly gridded values (biome/yearly averages of the map-data difference sampled at the location/time of the comparison data, Sect. 3.5.1).

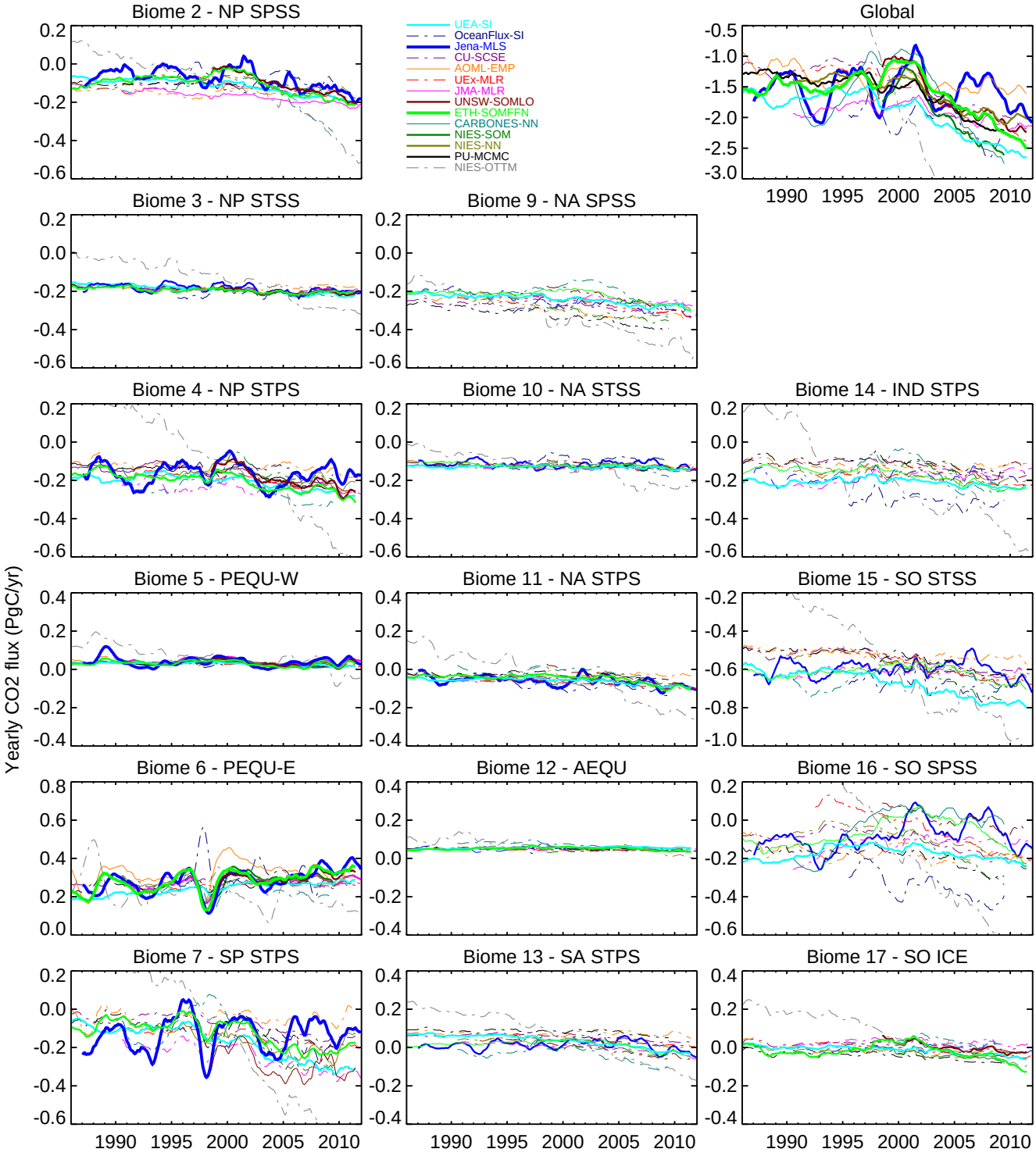


**Fig. A4.** Interannual variations of the sea–air $CO_2$ flux as estimated by all mapping methods, integrated over the biomes by Fay and McKinley (2014) (see Fig. 2, panels roughly in geographical arrangement). Line styles indicate the relative IAV mismatch: $R^{\mathrm{iav}} < 30\%$ (thick), 30–60% (medium), 60–75% (thin), above 75% (dashed); the legend reflects "Global". Vertical scales span the same range for all biomes ($0.8\,\mathrm{PgC\,yr^{-1}}$ except the global flux), but some vertical shift has been chosen according to the mean spatial flux pattern. In some biomes, lines of certain mapping methods with higher mismatches have been clipped (rather than enlarging the vertical scale), in order to maintain clarity. Biomes 1 (North Pacific Ice) and 8 (North Atlantic Ice) have been omitted due to extremely sparse data coverage.

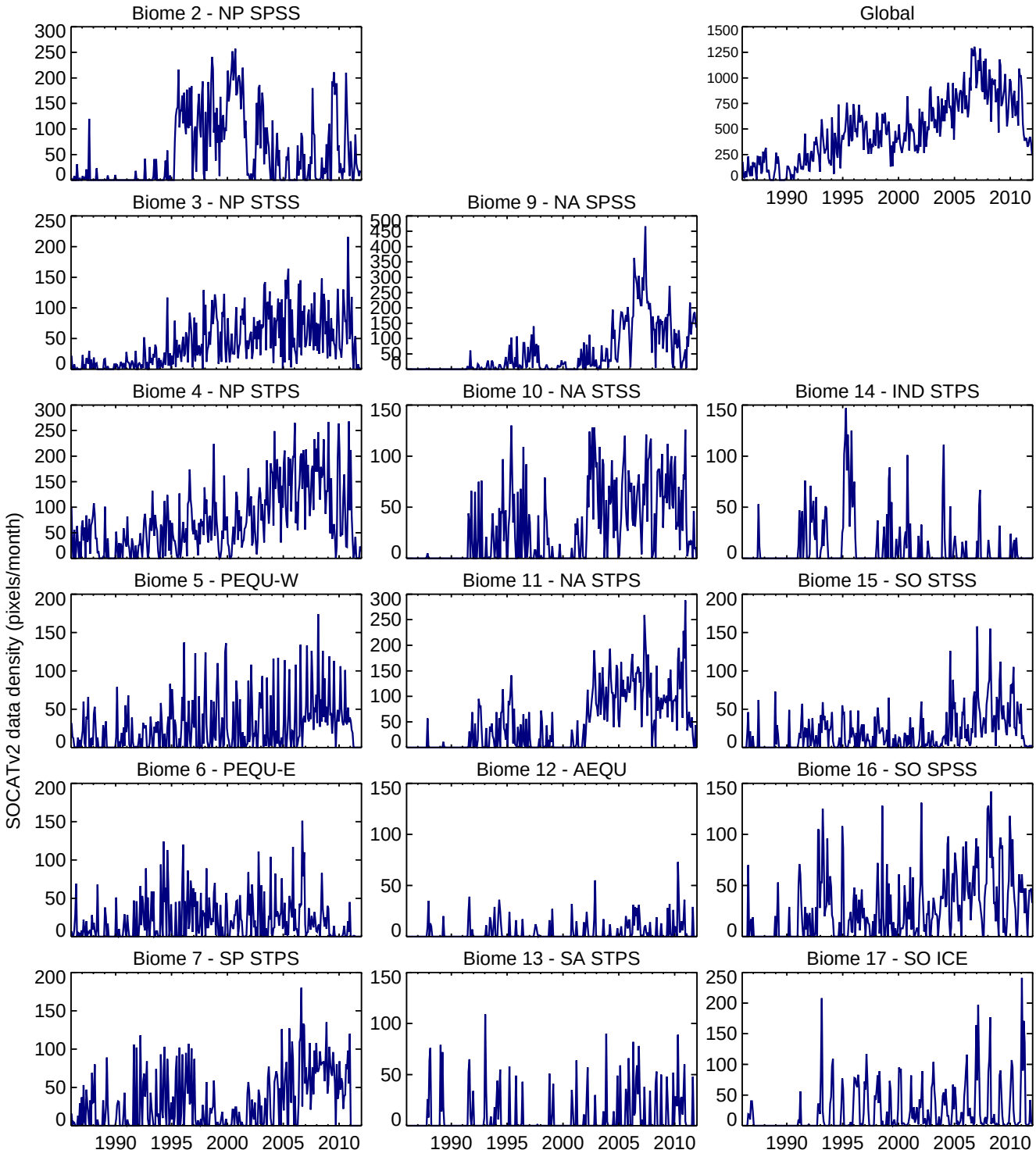


**Fig. A5.** Data density of the gridded SOCATv2 product used for comparison: Number of data-covered pixels per month in each biome. (Note that these values are only roughly indicative of the strength of data constraint, which not only depends on the number of data but also strongly on their distribution within the biome. Also, the magnitudes cannot be compared between biomes, because they have differently many pixels and the pixel size depends on latitude. Further note that several methods use LDEO or other SOCAT versions, thus may be constrained more strongly or more weakly in certain periods.)

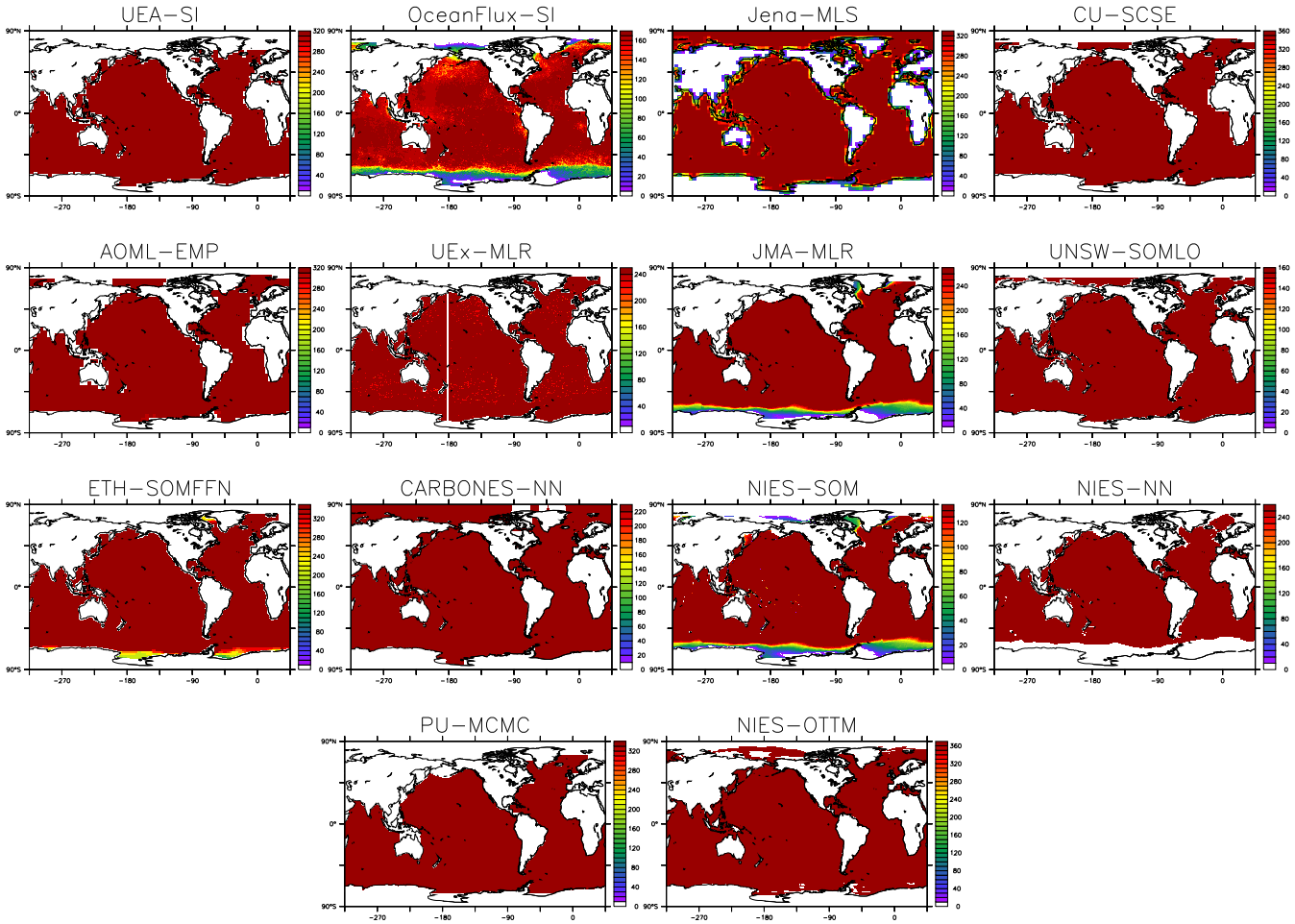


**Fig. A6.** Valid domain for each mapping method (colored area). The color gives the number of valid months within the period of the method; a number less than the maximum (dark red) indicates either (1) a fractional sea mask along coasts (*Jena-MLS*), (2) seasonally invalid months due to unavailable Chlorophyll-a input data (*JMA-MLR, ETH-SOMFFN, NIES-SOM*), or (3) occasional invalid months due to missing SST input (*OceanFlux-SI*) or numerical reasons (*UEx-MLR*).

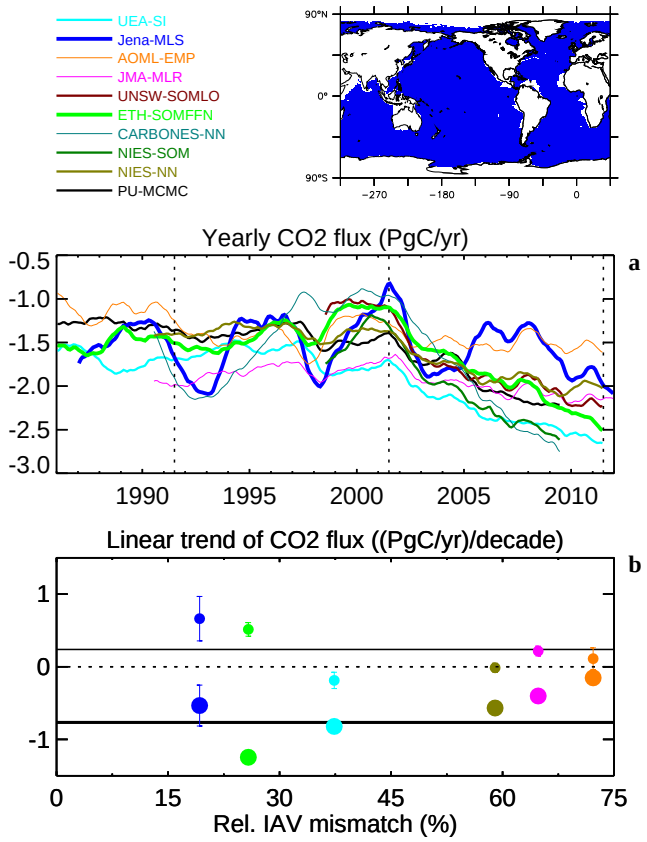


**Fig. A7.** Decadal sea–air $CO_2$ flux variations in the global ocean from selected mapping methods (having relative IAV mismatch $R^{\mathrm{iav}} < 75\%$ for globally averaged $pCO_2$). **(a)** Interannual time series as in Fig. 5(c). Line styles indicate the relative IAV mismatch: $R^{\mathrm{iav}} < 30\%$ (thick), 30–60% (medium), 60–75% (thin). The vertical dotted lines delimit the periods for the trend computation. **(b)** Linear trends over 1991–2001 (smaller symbols) and 2001–2011 (larger symbols) plotted against the relative IAV mismatch amplitude $R_i^{\mathrm{iav}}$ for each submission (cases not fully covering the two trend periods have been omitted to avoid inconsistencies). Error bars only reflect the uncertainty of the linear fit due to interannual variations (calculated assuming consecutive years to be statistically independent). Despite the very short periods, a more negative trend in the later period is a significant and consistent feature. The solid black horizontal lines give the weighted mean trends for the two periods, where submissions have been weighted both according to $R^{\mathrm{iav}}$ and to the uncertainty of the linear fit.